# MESOPOROUS CARBON DERIVED FROM *Hermetia illucens* PUPAE CASINGS AND BIOGAS SLURRY FOR CADMIUM REMOVAL FROM WATER BY CAPACITIVE DEIONIZATION METHOD

**Eva Panja**

**A Dissertation Submitted in Partial Fulfilment of the Requirements for the Award of the Degree of Master of Science in Materials Science and Engineering of the Nelson Mandela African Institution of Science and Technology**

**Arusha, Tanzania**

**June, 2025**

## ABSTRACT

This study examined capacitive deionization's effectiveness for recovering $Cd^{2+}$ from water using novel carbon-based electrodes derived from *Hermetia illucens* pupae casings (PC) and biogas slurry (BG). Activated carbon (AC) was produced through carbonization at 500°C and chemical activation (KOH) at 700°C. The Brunauer-Emmett-Teller method, Scanning Electron Microscope, X-ray diffractometer, Fourier transform infrared, X-ray photoelectron spectroscopy, Raman spectroscopy, and contact angle measurements were performed on AC. Electrochemical impedance spectroscopy and cyclic voltammetry were used to test the electrochemical properties of carbons. The PC-derived carbon (PC-2-700) had a specific surface area of 640 $m^2/g$, while the BG-derived carbon (BG-2-700) showed a higher 927 $m^2/g$. PC-2-700 exhibited a higher specific capacitance (271.9 $Fg^{-1}$) compared to BG-2-700 (105.8 $Fg^{-1}$), indicating better charge storage performance. The CDI cell containing the working electrodes in 5 and 10 mg/L $Cd^{2+}$ solution was used for $Cd^{2+}$ removal. The PC-2-700 electrode achieved 91 % removal efficiency (10.9 mg/g capacity) in 5 mg/L $Cd^{2+}$ solutions, outperforming BG-3-700 electrode (60% efficiency, 2.3 mg/g). Moreover, PC-2-700 also demonstrated better charge and energy efficiency, consuming only 0.65 and 0.07 $kWhm^{-3}$ versus BG-2-700's 0.24 and 0.93 $kWhm^{-3}$ at 5 mg/L concentration, respectively. The enhanced performance of PC-2-700 was due to its better capacitance, specific surface area, and porous structure on the surface. This study showed potential electrodes can be designed from pupae casings to remove heavy metals from water.

## DECLARATION

I, Eva Panja, declare to the Senate of Nelson Mandela African Institution of Science and Technology that this dissertation is my original work and has neither been submitted nor is concurrently submitted for a degree award at any other institution.

9/07/2025

Eva Panja Date

The above declaration is confirmed by:

9/07/2025

Prof. Yusufu Abeid Chande Jande Date

9/7/2025

Dr. Joyce Elisadiki Date

## COPYRIGHT

## CERTIFICATION

The undersigned certify that they have read and hereby recommend for acceptance and approval by the Senate of the Nelson Mandela African Institution of Science and Technology a dissertation titled "*Mesoporous Carbon Derived from Hermetia illucens Pupae Casings and Biogas Slurry for Cadmium Removal from Water By Capacitive Deionization Method*" in partial fulfilment for the requirements of the Award of the Degree of Master of Science in Materials Science and Engineering of the Nelson Mandela African Institution of Science and Technology, Arusha Tanzania.

9/7/2025

Prof. Yusufu Abeid Chande Jande Date

9/7/2025

Dr. Joyce Elisadiki Date

## ACKNOWLEDGEMENT

I am so grateful to my Almighty God, the creator, for giving me strength in this research. Second, my supervisor, Prof. Yusufu Abeid Jande Chande, deserves the most profound appreciation for his time, constant guidance, patience, insights, and personal skills throughout the research. I also appreciate my heartfelt thanks to Dr. Joyce Elisadiki for co-supervising this research. Her guidance, criticism, and directives in writing scientific papers and this dissertation are unforgettable. Special thanks to Dr. Tusekike Alfredy for her invaluable advice and admirable support; her encouragement during the ups and downs of my research progress printed a memory in my career. I also appreciate Mr. Omary Sufian, a PhD candidate, for his sincere support throughout my research. I acknowledge the technical support provided by NM-AIST laboratory technicians.

I sincerely thank Dar es Salaam University College of Education (DUCE) for granting me study leave and sponsoring my Master's studies. Without Duce's financial support, this study could be impossible to accomplish. The Nelson Mandela Institution of Science and Technology (NM-AIST) is also acknowledged for offering me a chance to study and allowing me to use their laboratories.

I honestly thank my family for everlasting support during my Master's studies. My father Mr. Joshua Panja, and my mother Ms. Mawazo Mwazembe have encouraged me through all my studies. Their contributions are irreplaceable in my life.

Words cannot express the boundless love, encouragement, moral support, and caring from my husband Mr. Peter Bulugu, my daughter Blessing Peter, and my son, Erick Peter. Their encouragement and ample time with me have motivated me to do my research.

## DEDICATION

I dedicate this work to my lovely husband Mr. Peter Bulugu, my daughter, Blessing Peter, my son, Erick Peter, and my parents, Mr. Joshua Panja and Ms. Mawazo Mwazembe.

**TABLE OF CONTENTS**

## LIST OF TABLES

## LIST OF FIGURES

## LIST OF ABBREVIATIONS AND SYMBOLS

| | |
|---|---|
| $v$ | Scan Rate |
| $\sum$ | Total Charge (c/g) |
| AAS | An Atomic Absorption Spectroscopy |
| AC | Activated Carbon |
| BET | Brunauer-Emmet-Teller |
| BG | Biogas Slurry-Derived Carbon |
| BG | Biogas Slurry |
| BGS | Biogas Generate Biogas Slurry |
| BGSC | Biogas Slurry Carbon |
| BG-X-Y | Biogas Slurry-Based Electrodes |
| BSF | Black Soldier Fly |
| C, F g-1 | The Electrode Capacitance |
| $Cd^{2+}$ | Cadmium Ions |
| $Cd_2Cl_4.5H_2O$ | Conductive Carbon Black, Activated Carbon, and Cadmium Chloride |
| CDI | Capacitive Deionization |
| Ci | Final Concentration |
| $C_i$ and $C_t$ | Initial and Final Concentrations of $Cd^{2+}$ ($mgL^{-1}$), |
| CV | Cyclic Voltammetry |
| E | Energy Consumption in kWhm-3 |
| EC | Electrosorption Capacity |
| EDL | Electric Double Layer |
| EIS | Electrochemical Impedance Spectroscopy |
| ESR | Equivalent Series Resistance |
| F | Faradays Constant |
| FTIR | Fourier Transform Infrared Spectrometer |
| HCl | Hydrochloric Acid |
| I | Current |
| IUPAC | International Union of Pure and Applied Chemistry |
| KOH | Potassium Hydroxide |
| NaOH | Sodium Hydroxide |
| NLDFT | Non-Local Density Function Theory |

| | |
|---|---|
| $C_o$ | Initial Concentration |
| PC PC | Pupae Case-Derived Carbon |
| PC-X-Y | Pupae Case-Based Electrodes |
| PTFE | Polytetrafluoroethylene |
| PVDF | Polyvinylidene Difluoride |
| Q | Assigned Flow Rate |
| RE | Removal Efficiency |
| Rs | Represents Solution Resistance |
| SEM | Scanning Electron Microscope-Energy Dispersion |
| SEM-EDX | Scanning Electron Microscopy-Energy Dispersive X-Ray Spectroscopy |
| t | Charging Time |
| TDS | Eliminate Total Dissolved Solids |
| V | Applied Voltage |
| WHO | World Health Organization |
| XPS | X-Ray Photoelectron Spectroscopy |
| XRD | X-Ray-Diffraction |
| Ω | Unit of Electrical Resistance, the Ohm |

# CHAPTER ONE

# INTRODUCTION

## 1.1 Background of the problem

Water pollution has become a universal issue caused by intensive human activities. Heavy metals in water sources are a significant problem, increasing rapidly in recent decades and reaching an alarming rate (Siddiqui & Pandey, 2019; Yinan *et al.*, 2017). Heavy metals like arsenic, zinc, nickel, lead, copper, and cadmium are released from activities like smelting or treatment of ores, mines, burning of petroleum products from fossil fuel, unloading industrial waste, the disposal of household waste, food packaging, the use of pesticides, and agricultural fertilizers (Maftouh *et al.*, 2023). Heavy metals are highly toxic, carcinogenic, mutagenic, and challenging to degrade; moreover, they are easy to accumulate, and their properties last long (Ma *et al.*, 2022). Therefore, once they enter the environment, they pollute water and soil, and they may get into human body through different mechanisms like the food chain, posing a serious health concern.

Drinking water containing heavy metals like cadmium beyond the permitted level can lead to health issues such as liver and kidney damage, decreased haemoglobin production, mental retardation, infertility, anaemia, renal degradation, skeletal abnormalities, persistent lung issues, and muscle cramps (Kacholi & Sahu, 2018; Peng *et al.*, 2016; Rwiza *et al.*, 2021). Cadmium components are classified as Group 1 carcinogens (Huang *et al.*, 2016). According to World Health Organization (WHO, 2014), the accepted level of cadmium in water is 0.003 $mgL^{-1}$. However, at low concentrations, cadmium is also a hazardous metal that has been linked to a higher risk of causing cancer (Rwiza *et al*., 2021).

Due increased in anthropogenic activities, Tanzanian water supplies from different areas have greater cadmium concentrations than the recommended limit (Table 1). For instance, it was discovered that the typical cadmium levels in Mara Rivers' water samples are 0.48 and 0.74 mg/L in the corresponding dry and wet seasons (Nkinda *et al.*, 2021). Water samples from the Kichangani swamp area in Morogoro have been reported to have a higher level of cadmium (0.06 mg/L) than accepted drinking water quality (Mdegela *et al.*, 2009). It is also noted, among others, that cadmium concentration in groundwater in Dar es Salaam is as high as 35 mg/L due to the impact of solid waste disposal (Kassenga & Mbuligwe, 2009). Moreover, groundwater in the Kahe catchment has been reported to have a cadmium concentration of 0.03 mg/L due to the intensive use of agrochemicals (Lwimbo *et al.*, 2019). A study by Mwegoha and

Kihampa (2010) showed that the cadmium concentration was higher, 0.01 $mgL^{-1}$, than the accepted level in the water of the valley of the Msimbazi River.

**Table 1: Concentration of $Cd^{2+}$ in selected surface water sources in Tanzania**

| Water sample | $Cd^{2+}$ concentration in mg/L | Reference |
|---|---|---|
| Mara Rivers | 0.74 | Nkinda *et al*. (2021) |
| Kichangani swamp area in Morogoro | 0.06 | Mdegela *et al*. (2009) |
| Groundwaters in Dar es Salaam | 35 | Kassenga and Mbuligwe (2009) |
| Kahe catchment area | 0.03 | Lwimbo *et al*. (2019) |
| Valley of Msimbazi River | 0.01 | |

This calls for innovative, environmentally friendly, cost-effective, and sustainable technologies for removing $Cd^{2+}$ from water for human usage (Chen *et al.*, 2020; Gong *et al.*, 2022). With the increasing demand for clean and safe water, various methods like physisorption, reverse osmosis, biosorption, and capacitive deionization have been established as the solution for heavy metal recovery from water since they can deliver high removal efficiency (Bandara *et al.*, 2020; Chen *et al.*, 2020; Pyrzynska, 2019; Wu *et al.*, 2021). However, these methods have advantages and limitations. For example, reverse osmosis is currently used in larger-scale water desalination. Yet, because of their high cost, sophisticated operation, and secondary contamination, most of these technologies' applications are hindered (Huang *et al*., 2016).

Capacitive deionization (CDI) is anticipated to be emerging method to overcome the challenges of the technologies above. Due to its relatively low energy usage, simple operation, and environmental friendliness, CDI has recently received much attention (Huang *et al.*, 2016). An energy consumption of about 0.4 kWh $m^{-3}$ was required to eliminate total dissolved solids (TDS) from brackish water (Jande, 2015). The CDI unit electrodes serve as vital components, and research are being done to develop new electrode materials to enhance CDI performance. The electrodes commonly employed in CDI are aerogel-based carbon, activated carbon, graphene, nitrogen-doped carbon, and nanostructured carbon cloth which are widely utilized in deionization capacitors (Peng *et al.*, 2016; Xu *et al.*, 2014). Graphene and Carbon aerogel match the requirements for CDI use; however, their use is limited by their expensive manufacture and purchase costs (Machunda *et al.*, 2009). Hence, many works focus on preparing inexpensive and sustainable electrodes for CDI application (Lado *et al.*, 2016).

Owing to its superior surface area, enhanced electric conductivity, intrinsic structures, heteroatoms functional groups, appropriate distribution of pore sizes, and inexpensive cost of synthesis, biomass has recently emerged as a competitive alternative source of carbon materials

(Song *et al.*, 2023). Tea waste has been prepared as a CDI electrode to eliminate fluoride and chromium from water (Gaikwad & Balomajumder, 2017). Chicken feather-based electrodes were developed to remove $Pb^{2+}$ from water using the CDI method (Alfredy *et al.*, 2019). Also, sugar can bagasse fly ash was prepared as electrodes for desalination application (Lado *et al.*, 2016). Also, using biomass for synthesizing carbon materials provides a new and suitable solution for managing solid waste (Alfredy *et al*., 2019; Elisadiki *et al.*, 2019; Zhao *et al.*, 2019).

This study has investigated the potential of using two biomasses from *Hermetia illucens* (black soldier fly) pupae casings and biogas slurry for developing CDI electrodes for $Cd^{2+}$ removal from water. *Hermetia illucens* (black soldier fly [BSF]) pupae casings contain chitin as an essential content of its exoskeleton, which is among the natural biopolymers containing a mixture of N–acetyl–D–glucosamine. This chitin has been of interest in various fields, such as the pharmaceutical sector, wastewater treatment, the food sector, and many more (Kaya *et al.*, 2016; Martínez *et al.*, 2014; Younes & Rinaudo, 2015; Zargar *et al.*, 2015). It has been reported that chitin can be a good source of carbon; it has almost 36.6 wt% carbon (Li *et al.*, 2020; Ratchai *et al.*, 2023; Zhang *et al.*, 2020). These properties can mimic its surface characteristics, such as surface charges, functional groups, hydrophilicity, and porosity (Waśko *et al.*, 2016). Pupae casing can become a suitable carbon source with many nitrogen groups, promising surface area, and high capacitance (Choirul *et al.*, 2024). A study by Purkayastha and Sarkar (2020) managed to produce biochar from BSF pupae casings with high nitrogen levels, which is challenging to get in materials of natural origin without surface modification. A study by Li *et al.* (2020) used black soldier-derived biochar in salt removal, and removal efficiency and sorption capacity were 87.23 % and 11.52 $mgg^{-1}$ respectively.

Biogas slurry can contain up to 0.5-2.5% N. Several studies have utilized biogas slurry in the production of activated carbon with high surface area, good electrochemical properties for supercapacitors, and adsorption of both organic and inorganic pollutants (Enock *et al.*, 2017; Qian *et al.*, 2022; Wang *et al.*, 2019; Yuan *et al.*, 2011). A study by Qian *et al.* (2022) synthesized biogas-residue-based activated carbons with a specific surface area of 1278 $m^2/g$ and high adsorption capacity for organic and inorganic pollutants removal from aqueous solution. Another study by Wang *et al.* (2019) developed activated carbon from biogas residue that has excellent electrochemical performance for super-capacitors with good specific surface area and pore sizes. Considering the similarities between CDI and supercapacitors, biogas

slurry carbon (BGSC) appear to be a promising activated carbon materials for creating an efficient CDI electrode in reducing heavy metals from an aqueous solution.

## 1.2 Statement of the problem

Heavy metals in water have worsened recently due to natural and human activities (Siddiqui & Pandey, 2019). Both human health and the natural ecological ecosystem are negatively impacted by cadmium-polluted water (Gong *et al.*, 2022). High levels of cadmium ions ($Cd^{2+}$) have been reported in water sources in the Kahe and Dar es Salaam catchments, with concentrations ranging from 0.03 mg/L to as high as 35 mg/L, respectively, which significantly exceed the World Health Organization (WHO) recommended limit of 0.003 mg/L for drinking water (Kassenga & Mbuligwe, 2009; Lwimbo *et al.*, 2019). These elevated $Cd^{2+}$ levels pose serious health risks, given their magnitude relative to the strict WHO guidelines. Numerous methods have been researched to lessen the quantity of heavy metals in water (Chen *et al*., 2020; Wu *et al*., 2021). Reverse osmosis is among the mature technologies to reduce heavy metals from water, and it has a high removal efficiency (Alvizuri-Tintaya *et al.*, 2023; Lumami *et al.*, 2022). Commercial membranes can be costly, have problems with excessive energy use, and can fail to remove heavy metals, including lead and arsenic effectively (Lumami *et al.*, 2022).

To overcome these challenges, CDI is proposed because it uses low energy consumption and is simple to operate. The effectiveness of the CDI method is measured by the materials of the electrodes utilized. Various activated carbon CDI electrode materials have recently been investigated for cadmium removal from water (Gong *et al.*, 2022). To further improve their performance in CDI, surface modification via chemical N-doping has been used to increase the electrode's capacity to eliminate heavy metals from water. This is attributed to a low level of heteroatoms in pristine biomasses, which tends to foster the material's electric conductivity, advance the surface hydrophilic property, speed up the ion transfer, and enable electrodes/solution interaction, thereby enhancing their electrosorption performance of CDI (Gao *et al.*, 2024; He *et al.*, 2020; Li *et al.*, 2020; Raj *et al.*, 2020). Despite the complicated doping process and the high cost of synthetic nitrogen-containing materials, various studies have focused on preparing heteroatom-doped electrodes from biowaste to increase the electrode's capacity for removing heavy metals from the aqueous solution via the CDI process (Hsu *et al.*, 2020; Rangaraj *et al.*, 2019; Wang *et al.*, 2024). Wang *et al.* (2024) reported a maximum removal efficiency of 82% for $Cd^{2+}$ removal of the prepared nitrogen-doped carbon material with a surface area of 798 $m^2/g$. A work by Rangaraj *et al.* (2019) reported a maximum

capacitance of 174.5 $Fg^{-1}$ for N-doped carbon from tamarind shells than undoped one (70.6 $Fg^{-1}$), which enhances its CDI performance.

Few studies have investigated the utilization of self-nitrogen-doped electrodes for CDI in recovering cadmium ions from water, and the performance was promising and comparable to the modified ones. A study by Truong *et al.* (2023) used electrodes made from sargassum hemiphylum in removing $Cd^{2+}$ by CDI and achieved an efficiency of about 74 %. In another study by Song *et al*. (2023), three biochar electrodes were prepared for cadmium recovery for the aqueous solution with a removal efficiency above 80%. This study has investigated the potential of using two biomasses from *Hermetia illucens* (black soldier fly) pupae casings and biogas slurry for developing CDI electrodes rich in the N-functional group for $Cd^{2+}$ removal from water.

## 1.3 Rationale of the study

The escalating global demand for clean water has been exacerbated by the rapid growth of industrial and agricultural sectors, leading to widespread water contamination. Cadmium, a toxic heavy metal, poses significant health risks when present in water sources. To address this challenge, innovative methods are necessary to provide safe and accessible water for all. Traditional water treatment technologies often require substantial energy inputs, making them unaffordable for many communities. In response, emerging technology like CDI offers promising removal efficiency. This method is more energy-efficient and cost-effective, potentially leveraging renewable energy sources.

## 1.4 Research objectives

### 1.4.1 General objective

The general objective of this study was to develop N-doped activated carbon electrodes derived from biogas slurry and pupae casings for removing cadmium from aqueous solution by CDI.

### 1.4.2 Specific objectives

(i) To investigate structural and electrochemical properties of activated carbon materials developed from biogas slurry and black soldier pupae casings.

(ii) To evaluate the performance of CDI electrodes based on activated carbon derived from biogas slurry and black soldier pupae casings in removing cadmium from an aqueous solution.

## 1.5 Research questions

This study intends to provide solutions to the following research questions:

(i) What are the structural and electrochemical properties of activated carbons derived from pupae casings and biogas slurry that enhance CDI performance?

(ii) What is the CDI electrodes' electrosorption capacity (mgg-1) derived from biogas slurry and pupae casings when removing cadmium from water?

## 1.6 Significance of the study

This study aims to explore nitrogen-rich CDI electrodes that remove cadmium ions from water developed from biowaste materials. Cadmium ($Cd^{2+}$) was chosen among heavy metals due to its high toxicity, environment persistance, and severe health risks even at trace levels, making its removal from water a critical priority. This study focuses on developing nitrogen-rich capacitive deionization (CDI) electrodes from biowaste materials *Hermetia illucens* (black soldier fly) pupae casings (PC) and biogas slurry (BG) because these are abundant, low-cost wastes are rich in nitrogen. They can be converted into porous carbons with functional groups that enhance heavy metal adsorption. Utilizing these biomass wastes promotes sustainable waste valorization and improves electrode properties such as conductivity and wettability. The CDI technology is selected for its energy efficiency, operational simplicity, and ability to selectively remove ions like $Cd^{2+}$ with regenerable electrodes, offering a greener alternative to conventional treatment methods. This approach aims to provide an effective, sustainable solution for cadmium contamination, integrating waste management and water purification to support environmental and public health goals.

## 1.7 Delineation of the study

This study aimed to prepare self-nitrogen carbon for removing cadmium from synthetic water using CDI. The study explores synthesis methods of Activated Carbon (AC), material characterization, and electrodes performance in terms of cadmium removal efficiency and electrosorption capacity. The dissertation is designed into five sections. Chapter one introduces the research objectives, rationale, and significance of the study and research questions. Chapter

two reviews existing literature on the status of heavy metals in water sources worldwide, existing literature on electrode materials for CDI and its efficiency in heavy metals removal, working principle of CDI technology, mechanisms for cadmium ion removal from water by porous carbon, existence of carbon materials derived from biomasses, and properties of black soldier pupae casings and biogas slurry activated carbon. Chapter three details the synthesis of activated carbon, characterization techniques, electrode fabrication, electrode electrochemical, and CDI test. Chapter four analyzes results, including porosity, surface morphology, elemental composition, and CDI experiment. Chapter five concludes with findings and recommendations. This study aimed to prepare AC with natural nitrogen functional groups, enabling the development of an economical CDI system for cadmium removal. While lab-scale results demonstrated the material's potential for scalable water treatment, further research is required to evaluate its performance in natural water and address gaps in selectivity. This work contributed to sustainable solutions for mitigating cadmium pollution in water by prioritizing low-energy CDI technology compatible with renewable energy sources.

# CHAPTER TWO

# LITERATURE REVIEW

## 2.1 Status of heavy metals in water

Water contamination by heavy metals is a significant global issue resulting from both human and natural activities. Sources of heavy metal pollution include agriculture, mining, fossil fuel combustion, waste disposal, untreated wastewater irrigation, and the use of pesticides and fertilizers (Mohammadi *et al.*, 2019). These contaminants degrade water quality and impact vegetation, the food chain, and human health. Numerous studies worldwide have reported heavy metal concentrations in drinking water that exceed accepted safety limits. For example, research in India found elevated levels of iron, cadmium, lead, and manganese in drinking water (Mawari *et al.*, 2022). Similar findings have been reported in Iran, where drinking water samples contained higher concentrations of cadmium, lead, and mercury (Ravanipour *et al.*, 2021), and in Bangladesh, where both groundwater and surface water were found to be contaminated with heavy metals (Deeba *et al.*, 2021). Review papers further highlight the widespread nature of this problem. In Nigeria, potable water sources were found to contain heavy metals above permissible limits (Ozoko *et al.*, 2022). In Nigeria, potable water sources contained heavy metals above permissible limits (Ozoko *et al.*, 2022). In China, six heavy metals (copper, cadmium, nickel, arsenic, mercury, and zinc) were detected at levels exceeding domestic standards (Wang *et al.*, 2021).

Other reviews confirm that developing countries are particularly affected, with most reporting heavy metal concentrations in drinking water above recommended thresholds (Chowdhury *et al.*, 2016; Mohanadas *et al.*, 2023). Additional studies underscore the health risks associated with heavy metal exposure. For instance, research in Nigeria revealed that most surface and groundwater sources used for drinking exceeded safe limits for heavy metals (Okafor *et al.*, 2023). High levels of arsenic, chromium, and cadmium have explicitly been linked to adverse health outcomes, including stunting in children (Oginawati *et al.*, 2023).

Water samples from the Karnaphuli River in Bangladesh have been found to contain four heavy metals, including arsenic, chromium, and cadmium (Ali *et al.*, 2016). Drinking water in Khorramabad, Iran was found to have lead, chromium, cadmium, and zinc above permitted amounts (Mohammadi *et al.*, 2019). The Dzindi River in South Africa and river streams in Tanzania have been reported to contain various heavy metals, including iron, aluminium,

manganese, zinc, copper, lead, mercury, and arsenic (Edokpayi *et al.*, 2014). A study by Kacholi and Sahu (2018) reveals high levels of iron, zinc, lead, and copper in water samples of Temeke District in Dar es Salaam used for vegetable irrigation. Additionally, a study by Nkinda *et al*. (2021) finds that water from the chosen river streams of Mara River in Tanzania has the highest quantities of lead, mercury, chromium, cadmium, and arsenic. These studies consistently highlight cadmium as a widespread contaminant in water bodies, requiring affordable, efficient treatment technologies like CDI.

## 2.2 Mechanisms for cadmium ions removal from water by porous carbon

Removing $Cd^{2+}$ from an aqueous solution may involve three mechanisms: Complex formation, sharing electron pairs with nitrogen groups, and ion exchange, as shown in Fig. 1. The possible interaction of various functional groups with $Cd^{2+}$ during electrosorption may include:

(i) C=O

Oxygen in the carbonyl group can coordinate with $Cd^{2+,}$ forming a complex compound:
$R\text{-}COOH + Cd^{2+} \rightarrow R\text{-}COO^{-}.Cd^{2+}$

(ii) Amino group ($C\text{-}NH_2$)

The lone pair of electrons in the nitrogen can interact with $Cd^{2+}$ to form a coordination complex:

$R\text{-}NH_2 + Cd^{2+} \rightarrow R\text{-}NH_2.Cd^{2+}$

(iii) Hydroxyl group (C-OH)

Oxygen's lone pair of electrons can bind $Cd^{2+}$ :

$R\text{-}OH + Cd^{2+} \rightarrow R\text{-}O\text{-}Cd^{2+}$

(iv) Ester (C-CO-C) can participate in interaction to coordinate with metal ions.

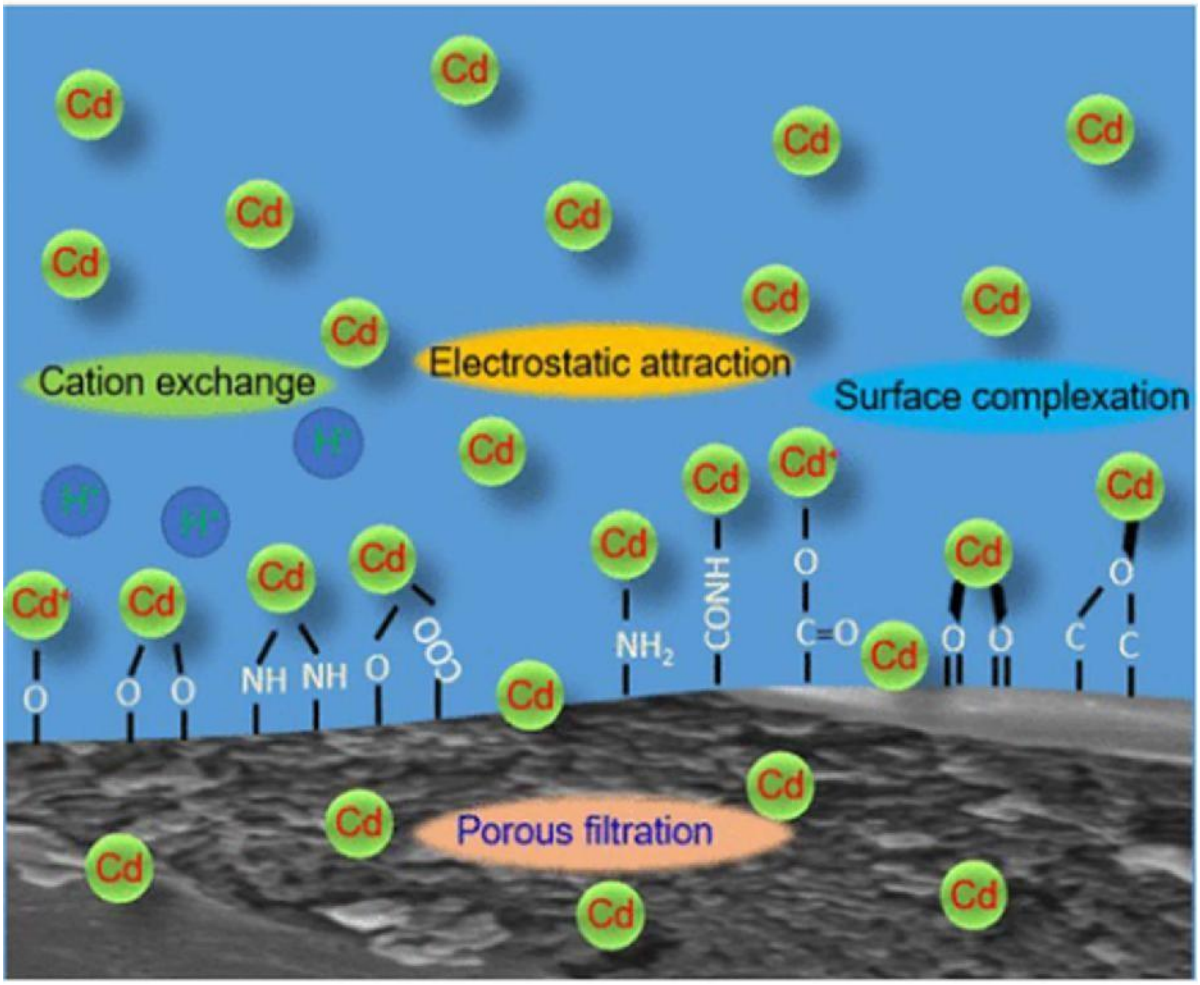


**Figure 1: Mechanisms for cadmium ions removal from water by porous carbon (Guo *et al.*, 2017)**

### 2.3 Chemistry of hetero-N-atom in the carbon structural matrix

The presence of hetero-nitrogen atoms, such as pyridinic-N and pyrrolic-N, in the carbon matrix significantly enhances electrosorption capabilities in capacitive deionization (CDI) systems. Pyridinic nitrogen, typically found at the edges of graphene-like structures, donates lone pair electrons that increase the local electron density, thereby creating Lewis basic sites which improve the adsorption affinity toward metal ions like $Cd^{2+}$ (Wang *et al.*, 2018). Pyrrolic nitrogen, integrated within five-membered rings, introduces redox-active sites that contribute to pseudocapacitive charge storage, enhancing the overall capacitance of the electrode (Liu *et al.*, 2017). Furthermore, nitrogen contents modify the surface chemistry by increasing hydrophilicity and wettability, facilitating better electrolyte penetration and ion transport within the porous carbon structure (Lu *et al.*, 2022). These nitrogen functionalities also induce structural defects and edge sites that serve as active centres for ion adsorption while maintaining the stability and electrical conductivity of the carbon framework (Enock *et al.*,

2017). Collectively, these effects improve charge transfer kinetics and ion binding, leading to enhanced electrosorption efficiency and electrode durability in CDI applications.

## 2.4 Working principle of CDI technology

Compared to other traditional desalination procedures, CDI is a recently developed and widely desirable approach because it is eco-friendly, has low energy usage, and is ease to regenerate and maintain (Peng *et al.*, 2016). The CDI is an electrosorption process involving the ions absorbed from an ionic solution on the surface of the electrode materials under an electric field. Positively charged ions such as calcium and cadmium are adsorbed onto an electrostatic double layer of electrodes negatively charged (cathode) when water is passing between the electrodes, while negatively charged ions such as chlorine adsorb onto the EDL of the electrodes positively charged (anode). Once electrodes have reached their adsorption capacity, adsorbed ions can be freed from electrode materials by discharging the cell at 0.0 V or polarity reversing of the cell (Gong *et al.*, 2022).

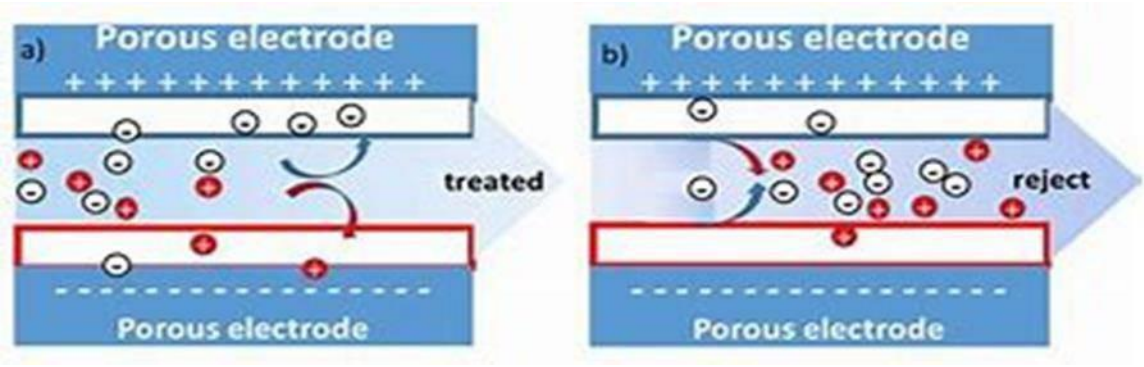


**Figure 2: Example of the CDI process showing the steps for (a) Ion elimination and (b) Electrode regeneration**

## 2.5 Electrodes materials for CDI and its efficiency in heavy metals removal

Specific surface area, conductivity, specific capacitance, and pore size distribution as structural characteristics of electrode materials typically determine CDI performance. Better conductivity and relatively large specific surface area contribute to improved adsorption capacity (Lin *et al.*, 2022). As a result, the creation and manufacturing of improved electrode materials have received much attention in CDI research. The effectiveness of removing cadmium from an aqueous solution using carbon materials in CDI is summarized in Table 2.

**Table 2: Electrode materials utilized in CDI pfor cadmium removal from water**

| Materials | $\mu$% | EC (mg/g) | Initial concentration ($mgL^{-1}$) | V (v) | Time (h) | Volume | Flow rate ($Mlmin^{-1}$) | Approach | Size of electrodes | References |
|---|---|---|---|---|---|---|---|---|---|---|
| Activated carbon cloth | 32 | 103.6 | * | 1.2 | * | * | 0 | Batch mode | One by one inch | Huang *et al.* (2016) |
| Activated carbon powder | 93 | * | 100 | 1.2 | 3 | * | 20 | Batch mode | * | Gong *et al.* (2022) |
| Birnessite activated electrodes | * | 900 | 200 | * | 2 | * | * | Batch mode | * | Peng *et al.* (2016) |
| N-doped Biochar Humic acid. | 89 | 79 | 4 | 1.2 | 2 | * | | Batch mode | * | Lin *et al.* (2022) |
| $MoS_2$/AC nanosheet composite | 58.06 | 22.15 | 0.001 | * | * | * | * | Batch mode | * | Yin *et al.* (2022) |

## 2.6 Based materials derived from biomass

Because biomass and agricultural residue have an ample supply of raw materials, better electrical conductivity, low production costs, and a promising specific area, they have recently received a lot of attention as possible new sources of carbon precursors (Lado *et al.,* 2016; Zhu *et al.,* 2018). Since it is valued at a low cost and is a renewable resource that is good for the environment, biomass is a good raw material (Song *et al.,* 2023).

To make CDI electrodes, several biomass materials can be employed as a precursor, including coconut shells, cattle manure, coconut shells, rice husk, sugarcane bagasse, and tea waste (Deng *et al.,* 2021; Farma *et al.,* 2023; Ramalingam *et al.,* 2020). Lately, studies have investigated waste suitability as electrode materials in CDI applications.

Activated carbon from biomass waste from tea is used as CDI electrodes to remove fluorine and carbon. For a 10 mg/l mix feed solution, the removal percentages were determined to be 88.5 and 85.20%, respectively (Gaikwad & Balomajumder, 2017). Additionally, it is stated that carbonized sorghum stem-derived carbon has been employed as super-capacitors and CDI electrodes, exhibiting notably larger capacitance (257 $Fg^{-1}$) and BET surface area (1347 $m^2g^{-1}$) (Kim *et al.,* 2021). Citrus-activated carbons were used as the anode in a CDI cell using a hydrothermal synthesis method and showed a suitable specific capacitance of 120 F/g. Moreover, prepared soybean shell-based activated carbon via pyrolysis approach shows a high surface area of 1032.2 $m^2g^{-1}$, an adsorption capacity of 15.5 mg/g at an absorption rate of 0.44 $mgg^{-1}$ $min^{-1}$ at 1.2 V performed well in CDI methods (Zhao *et al.,* 2018). These few pieces of research support the idea that bio-waste, which is abundant, inexpensive, and environmentally beneficial, can be assessed for use in CDI electrodes to remove heavy metals.

## 2.7 Properties of biogas slurry activated carbon

Plants that produce biogas generate biogas slurry (BGS) as a waste product. The 0.5-2.5% N is present in a range of BGS made using various production methods (Surendra *et al.,* 2014). The differences in the nutritional makeup of BGS can be attributed to the biochemical constituents of feedstock and the circumstances under which it is generated. For example, the N content of solid animal manure could vary from 0.4 to 0.8% depending on the storage and feed circumstances (Surendra *et al.,* 2014). For instance, Khan *et al.* (2014) described the BGS as containing more nitrogen than the feedstock made from solid animal feedstock. A work by Yuan *et al.* (2011) utilizes biogas residue as activated carbons for organic and inorganic waste

adsorption. The findings illustrate the practical synthesis of activated carbons with a specific surface area (1950 $m^2/g$) and pore volume (1.232 $cm^3/g$) was achieved. Qian *et al.* (2022) synthesized biogas-residue-based AC with a specific surface area of 1278 $m^2/g$, high adsorption capacity for organic and inorganic pollutants removal from water. Another study by Wang *et al.* (2019) developed AC from biogas residue that has excellent electrochemical performance for super-capacitors with good specific surface area and pore sizes was attained. The outcomes verify that excellent electrochemical cycle stability and high specific capacitance were attained.

A supercapacitor with a larger surface area of 350 $m^2/g$, capacitance of 289 $Fg^{-1}$, and 3-4.5 nm fine pore distribution was made using biogas slurry carbon (BGSC) chemically activated with a KOH/BGSC volume proportion of 2:1 (Enock *et al.*, 2017). Considering the similarities between CDI and supercapacitors, BGACs are a promising activated carbon material for creating an efficient CDI electrode to reduce heavy metals from an aqueous solution. The BGACs have shown large surface area, noble pore structure, good conductivity, and the presence of oxygen and nitrogen functional groups in supercapacitors. This work aimed to develop activated carbon materials for creating CDI biogas slurry-based electrodes and evaluate the degree of cadmium removal.

### 2.8 Properties of black soldier pupae casings activated carbon

The BSF larvae are insects that have been most recently studied. They are produced on a massive scale worldwide and are used as a source of chitin and animal feed rich in protein and fat (Choirul *et al.*, 2024; Soetemans *et al.*, 2020). During the breeding stage, some percentage are left to be converted to flies for laying eggs, leaving shells as waste when molting out. Pupae case is rich in chitin. Chitin is a naturally occurring fiber-formamide. Pupae casing can become a suitable carbon source with many nitrogen groups, promising surface area, and high capacitance (Choirul *et al.*, 2024). Pupae casing has been used as an adsorbent of methylene blue dye, and the removal efficiency was 96.1 % (Choirul *et al.*, 2024). A study by Li *et al.* (2020) used BSF chitin-derived biochar in salt removal, which had efficiency and sorption capacity of 11.52 $mgg^{-1}$ and 87.23 %, respectively. A study by Purkayastha and Sarkar (2020) produced biochar from BSF pupae casings, which have high nitrogen levels and are difficult to get in materials of natural origin without surface modification. To date, no studies have researched the possibility of using carbon from BSF pupae cases as electrode material for heavy metal removal by CDI.

# CHAPTER THREE

# MATERIALS AND METHODS

## 3.1 Materials

The *Hermetia illucens* (black soldier fly) pupae casings and biogas slurry were collected from animal nutritious food production and biodigester in Seela village in Sing'isi ward, Meru district, Tanzania. Chemicals, including polytetrafluoroethylene (PTFE), were bought from Sigma-Aldrich, Sodium Hydroxide (NaOH), Hydrochloric acid (HCl), and Potassium Hydroxide (KOH) were purchased from Merk company, India. These chemicals were used without modification since they were in analytical grade. Conductive carbon black, activated carbon, and cadmium chloride ($Cd_2Cl_4.5H_2O$) were collected from Shandong Richnow Chemical Co., China.

## 3.2 Carbonization and activation process of biogas slurry and pupae casings precursor

Preparation of activated carbons was done as shown in Fig. 3. Specifically, the following procedures described by Enock *et al.* (2017) were followed. Black soldier fly pupae cases were washed, dried for 12 hours, and crushed to ~160 μm particles. Biogas slurry was air-dried for five days. Each material (30 g) was carbonized in a nitrogen atmosphere at 500°C for 1 hour with a 10°C/min ramp rate. Pre-carbonized samples were chemically activated with KOH (1:1, 1:2, and 1:3 ratios) at 700°C for 2 hours under nitrogen gas (Fig. 3). After natural cooling, carbons were washed with 1 M HCl until neutral pH and dried at 100°C for 12 hours, labelled PC-700 and BG-700.


**Figure 3: Schematic description of the synthesis of carbon from biogas slurry and pupae casings**

### 3.3 The CDI electrodes preparation

The procedures for preparing CDI electrodes were adopted from Alfredy *et al.* (2019) and Elisadiki *et al.* (2020). The activated sample, polytetrafluoroethylene (PTFE), and carbon black were combined in the presence of ethanol solution at a mass proportion of 8:1:1 at room temperature to create a dough-like paste, which was then rolled to a suitable size and cut into 4 cm by 4 cm squares. The dough was then processed at 50°C for 10 hours to act as the working electrode material, with a total mass of approximately (200 mg – 210 mg) (Fig. 4). The prepared electrodes were denoted as PC-X-Y for the pupae case-based electrodes, and BG-X-Y for biogas slurry-based electrodes, where X is KOH ratio, and Y is activation temperature.

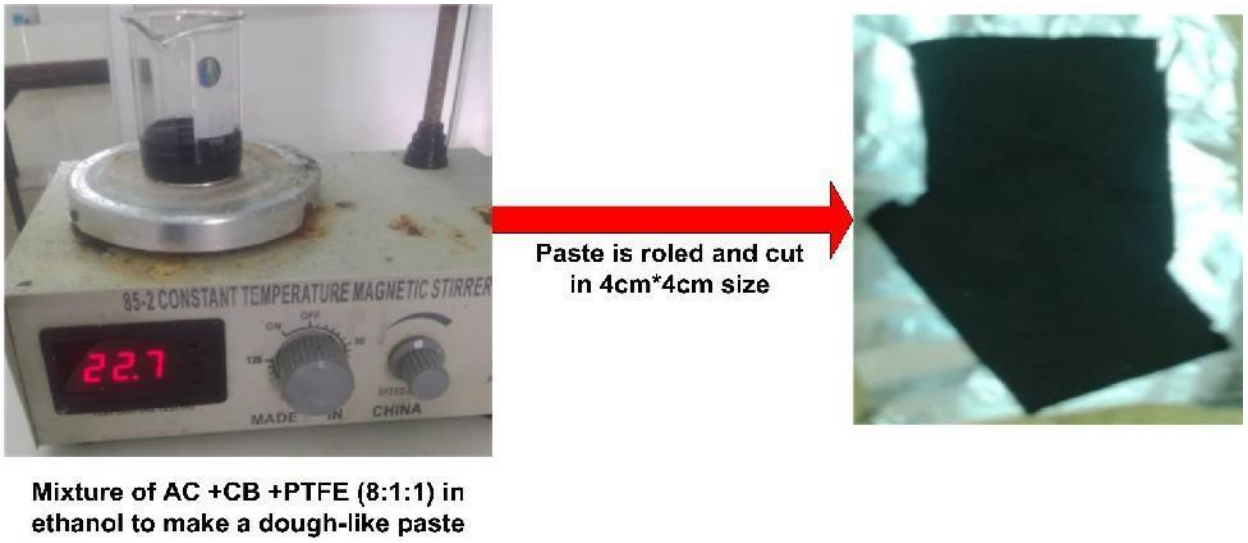


**Figure 4: Preparation of CDI electrodes**

### 3.4 Characterization of the prepared activated carbons

Scanning electron microscopy (SEM, Carl Zeiss Ultra Plus) was used to analyse the surface morphological structure of the materials. The Porosimeter, 1994-2017 Quantachrome instrument was used to determine Nitrogen adsorption/desorption isotherms at 77.35 K in the relative pressure ($p/p_o$) of 0.99 to estimate the specific surface area of the activated carbons. The prepared samples were firstly outgassed in a vacuum at 300°C for 1 hour. Non-Local Density Functional Theory (NLDFT) methods were used to determine the pore size distribution of activated samples. The analysis of functional groups on the surface of materials using an FTIR (Fourier transform infrared spectrometer, FTIR Shimadzu IRSpirit-A224159). The diffraction patterns of activated carbon were conducted using an XRD (X-ray diffractometer, Bruker D8 Advance diffractometer). The existence of nitrogen content was confirmed with X-ray photoelectron spectroscopy (XPS). The properties and structure of carbon were analyzed

using Raman spectroscopy. Materials contact angles were measured using a contact angle goniometer (L 2004A-0388).

### 3.5 Electrochemical test of electrodes

The electrochemical properties of activated carbons, which were determined by electrochemical impedance spectroscopy (EIS) and cyclic voltammetry (CV) tests, were determined by PGSTAT204, AUT50663 Metrohm as a working station. The electrolyte concentration used for the EIS and CV test was 6 M KOH. The Ag/AgCl electrode serves as the working electrode, reference electrode, and counter electrode in a three-electrode working system. The EIS test was conducted using a frequency range of 0.01 Hz to 100 000 Hz and an amplitude of 10 mV. The preparation of electrodes for electrochemical properties adopts the procedures described in Enock *et al.* (2017). The employed electrode was created by pushing a mass load of about 5 mg active material as a mixture of activated carbons, polyvinylidene difluoride (PVDF), and conductive carbon at a mass ratio of 8:1:1 on two pieces of nickel foam. The electrode Capacitance (C, F g-1) based on the CV curves was estimated using the formulae Equation (1).

$$C = \int_{v_i}^{v_f} \frac{I}{rm\Delta V} du \quad (1)$$

Whereby, I (A) is response current, r ($Vs^{-1}$) is potential scanning rate, ΔV is a potential window, and m is mass active material deposited on the electrode.

### 3.6 Electrosorption of $Cd^{2+}$ with CDI

Two $Cd^{2+}$ ion concentrations (5 mg/L and 10 mg/L) were prepared from $CdCl_2$ salt. An electrosorption investigation of $Cd^{2+}$ was done with a lad scale CDI cell with PC-700 and BG-700 in batch mode at a 10 mL /min circulating rate. A voltage of 1.2 V was applied to the CDI cell using potentiostat/galvanostat (1A. EIS 1A/10 V/1 MHz EIS, Ivium Technologies, The Netherlands, equipped with Iviumsoft electrochemistry software). An initial solution volume of 30 mL was supplied in the cell using a peristaltic pump for 90 minutes. After every 5 seconds, the conductivity meter (GMH 3400) was used to monitor the conductivity of the solution to predict the removal efficiency. An Atomic Absorption Spectroscopy (AAS-WFX210) determined the $Cd^{2+}$ concentration.

Equation (2) and (3) illustrated the calculation of removal efficiency (RE) and electrosorption

capacity (EC) of $Cd^{2+}$ from the solution, respectively.

$$RE = \frac{C_o - C_f}{C_o} \times 100\% \quad (2)$$

$$CE = \frac{C_i - C_t}{m} \times V \quad (3)$$

Whereby, V is the volume used of the solution (mL), $C_i$ and $C_t$ are the initial and final concentrations of $Cd^{2+}$ ($mgL^{-1}$), respectively, and m is the mass of the electrode (g).

The electrodes' energy consumption and charge efficiency were calculated to estimate CDI performance in removing $Cd^{2+}$ from water.

$$\Lambda = \frac{F \,.\, \Gamma}{M_W \,.\, \Sigma} \quad (4)$$

$$E = \frac{V \int_o^t I dt}{Qt} \quad (5)$$

Whereby, E is energy consumption in $kWhm^{-3}$, V is applied voltage, I is current, Q is assigned flow rate, t is charging time, F is faradays constant (96485 c/mol), $\sum$ is a total charge (c/g) obtained by integrating current curve, and its electrosorption capacity.

# CHAPTER FOUR

# RESULTS AND DISCUSSION

## 4.1 Textural structure and surface morphology

Scanning electron microscope-energy dispersion (SEM) micrographs for the surface and pore morphologies of prepared PC carbons are shown in Fig. 5. Without carbonization, the surface of black soldier fly pupae casings tends to have organized repeated units of hexagonal/square boxes and non-porous structures, as earlier observed by Purkayastha and Sarkar (2020) and Soetemans *et al*. (2020). The PC carbon at a ratio of 1:1 (PC-1-700) presented the formation of a fluffy and less porous structure after high-temperature activation (Fig. 5a). The increase in KOH in PC-2-700, has resulted in the formation of sections of organized repeated units of hexagonal microfibrillar boxes on the surface (Fig. 5b). Also, in Fig. 5b, the depth of the holes in the boxes has increased, creating suitable pores that are beneficial for the electrosorption of heavy metals. This enhanced depth was due to a more extensive etching effect from KOH, which enlarges and deepens the pores. Pores are formed in Fig. 5c, and hexagonal boxes are destroyed on the PC-3-700 surface. This may be attributed to the contribution of a large amount of KOH, which reacted with the exterior and interior surfaces of the PC-3-700.

The SEM micrographs of BG carbons are depicted in Fig. 6. The smooth and less porous surface is observed in BG-1-700 due to a small amount of activating agent (KOH) (Fig. 6a). Whereas Fig. 6c-d shows a flake-like morphology on the surface of BG-2-700 with a lack of well-formed pores. This may be due to the complex properties of biomass feedstock for BG samples, which also affects the KOH activation process in achieving the desired structural characteristics and, hence, does not create significant porosity in BG-2-700. An increase in the amount of KOH results in many pores on the surface of BG-3-700, as shown in Fig. 6c, than in BG-1-700 and BG-2-700. In addition, the Scanning electron microscopy-energy dispersive X-ray spectroscopy (SEM-EDX) analysis and elemental mapping confirmed the existence of nitrogen, carbon, and oxygen content on the surface of the PC and BG samples (Fig. 7).

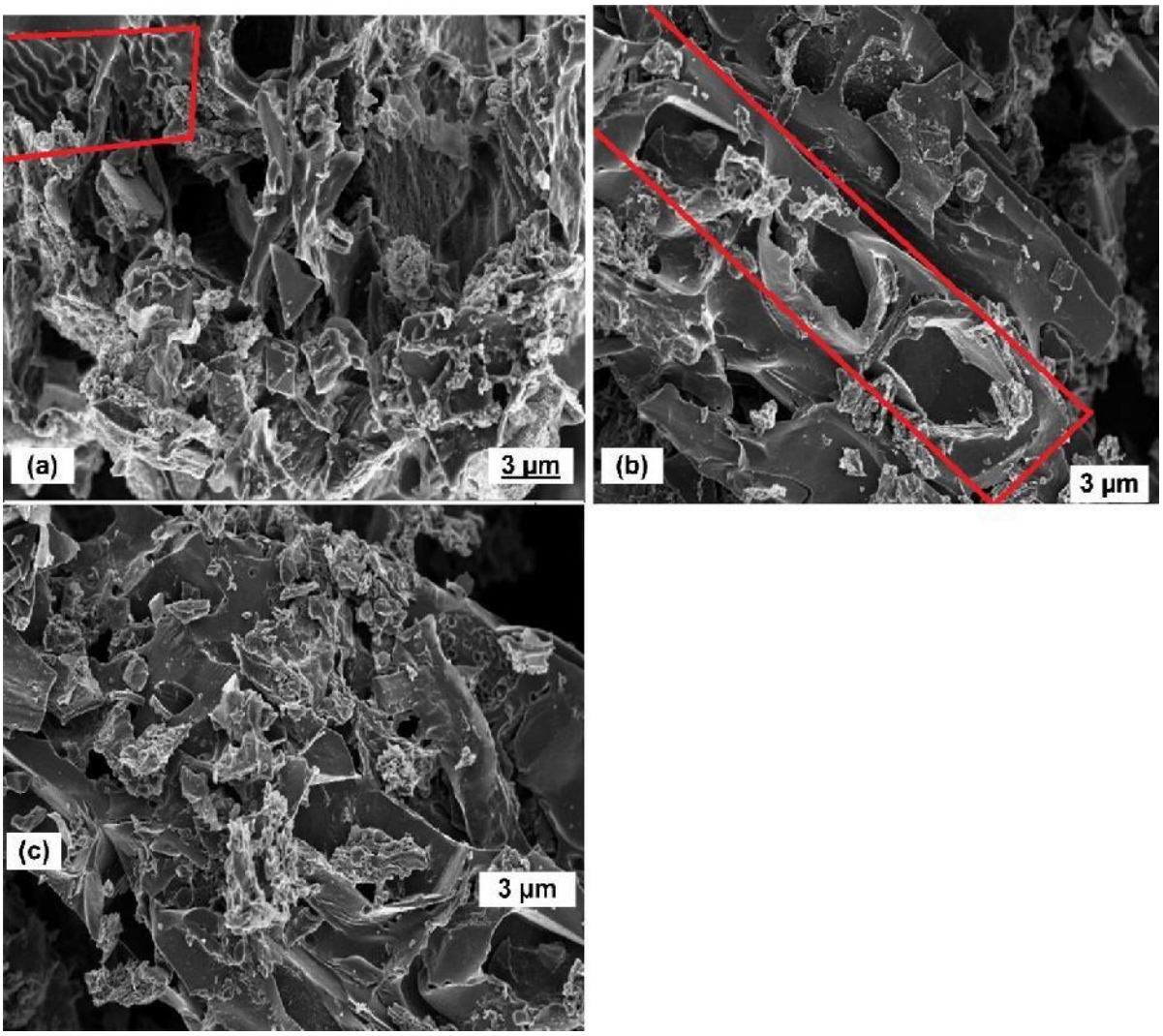


**Figure 5:** **The SEM images of PC samples showing development of porosity with increasing KOH ratios (a) PC-1-700 (b) PC-2-700 (c) PC-3-700**

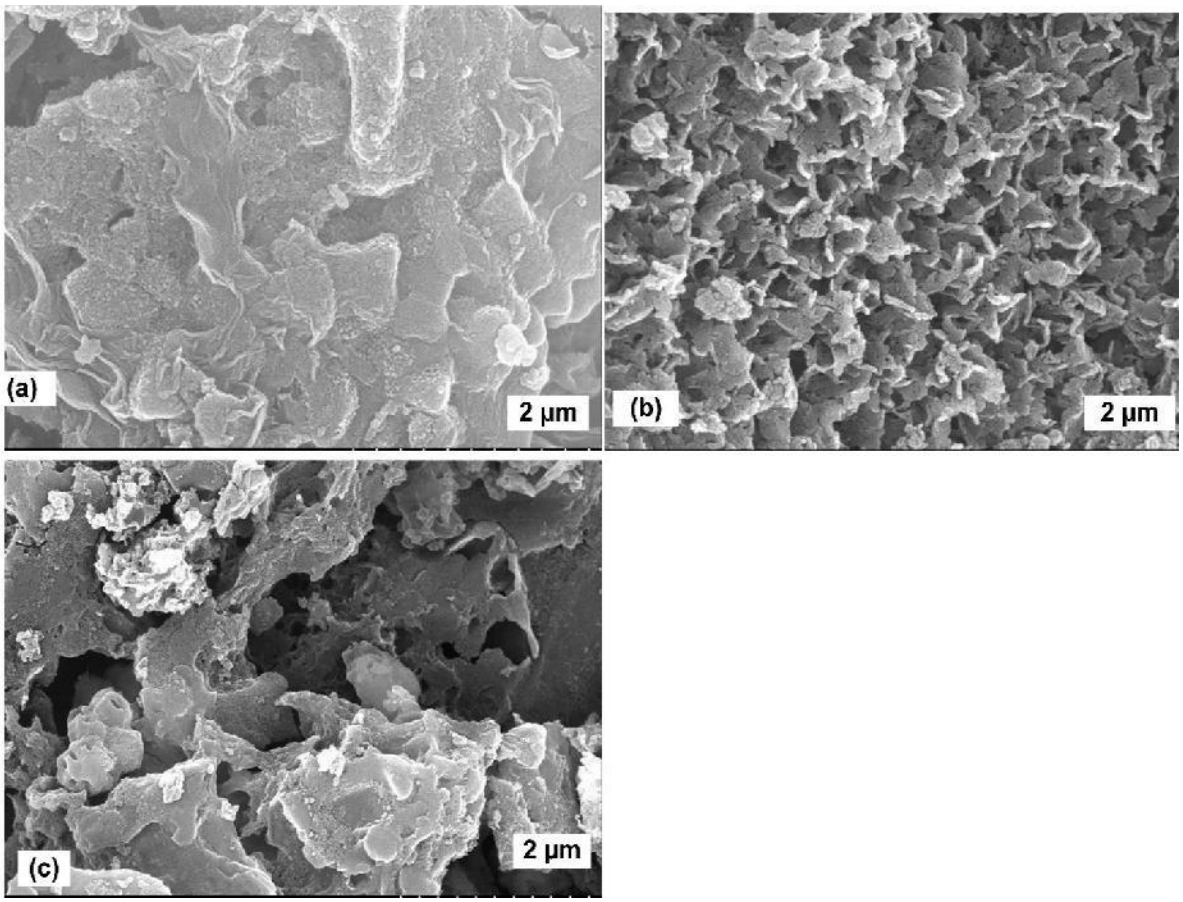


**Figure 6: The SEM images of BG carbon illustrating the differences in surface morphology at three KOH ratios (a) BG-1-700 (b) BG-2-700 (c) BG-3-700**

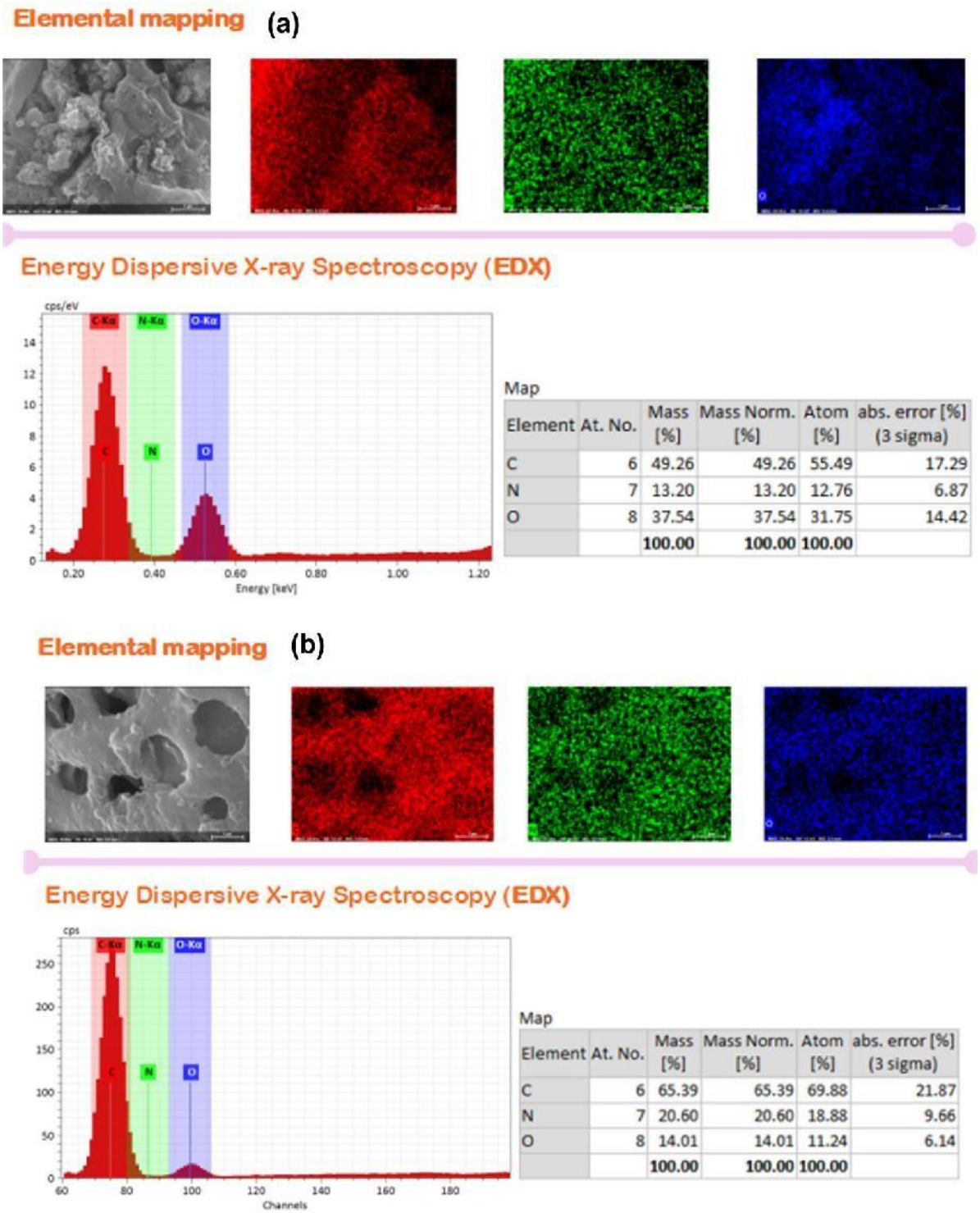


**Figure 7: (a) The SEM-EDX and elemental mapping for BG sample (b) PC sample**

## 4.2 Nitrogen adsorption/desorption analysis

Among the crucial factors affecting the adsorption capacity of electrodes are pore size distribution within the materials and the specific surface area (Fig. 8), illustrates Nitrogen adsorption/desorption Isotherms for PC and BG to characterize the carbon electrodes'porous structure and surface area. It is observed that all the adsorption isotherms for PC carbons belong

to type IV adsorption isotherms based on the classification of the International Union of Pure and Applied Chemistry (IUPAC) by showing the existence of a hysteresis loop at p/po greater than 0.4. This reveals that most PC carbon pores are mesopores with an average pore diameter of 3.3 nm. The $N_2$ adsorption isotherm for BG carbons is also a type IV isotherm with more micropores than mesopores. This is evidenced by an observation showing a slight steep increase in $N_2$ adsorption in the low-pressure zone in all BG isotherms showing the presence of micropores see (Fig. 8c). The NLDFT pore size distribution of all carbon is shown in Fig. 8b. Pore sizes mainly range below 2 nm for BG and above 2 nm for PC carbon. This implies many micropores in BG samples, as depicted in SEM images (Fig. 6a, b, and c). Therefore, the total surface area of activated carbon was calculated using the Brunauer-Emmet-teller (BET) model. Table 3 indicates the textural properties such, as pore size distribution, BET surface area ($S_{BET}$), and pore volume of prepared carbons.

The BG carbon possesses the largest specific surface area compared to other samples (Table 3). This is due to the availability of micropores in BG's carbon, which are associated with a highly specific surface area, as seen in the pore size distribution (Fig. 9d). The hydrated ionic radius of $Cd^{2+}$ (0.426 nm) may probably not match most of the micropores present in BG electrodes, resulting in considerable transport resistance and lower removal efficiency despite its highest surface area (Chen *et al.*, 2018; Song *et al.,* 2023). The existence of mesopores favors high electrosorption of $Cd^{2+}$, proving that mesoporouss enhance the contact of the $Cd^{2+}$ with PC electrodes and hence promote adsorption and transportation of $Cd^{2+}$ compared to BG electrodes. Availability of mesopores and larger surface area are essential in creating double-layer capacitors and may enhance the CDI electrosorption mechanism (Song *et al.,* 2023; Zhao *et al.,* 2019).

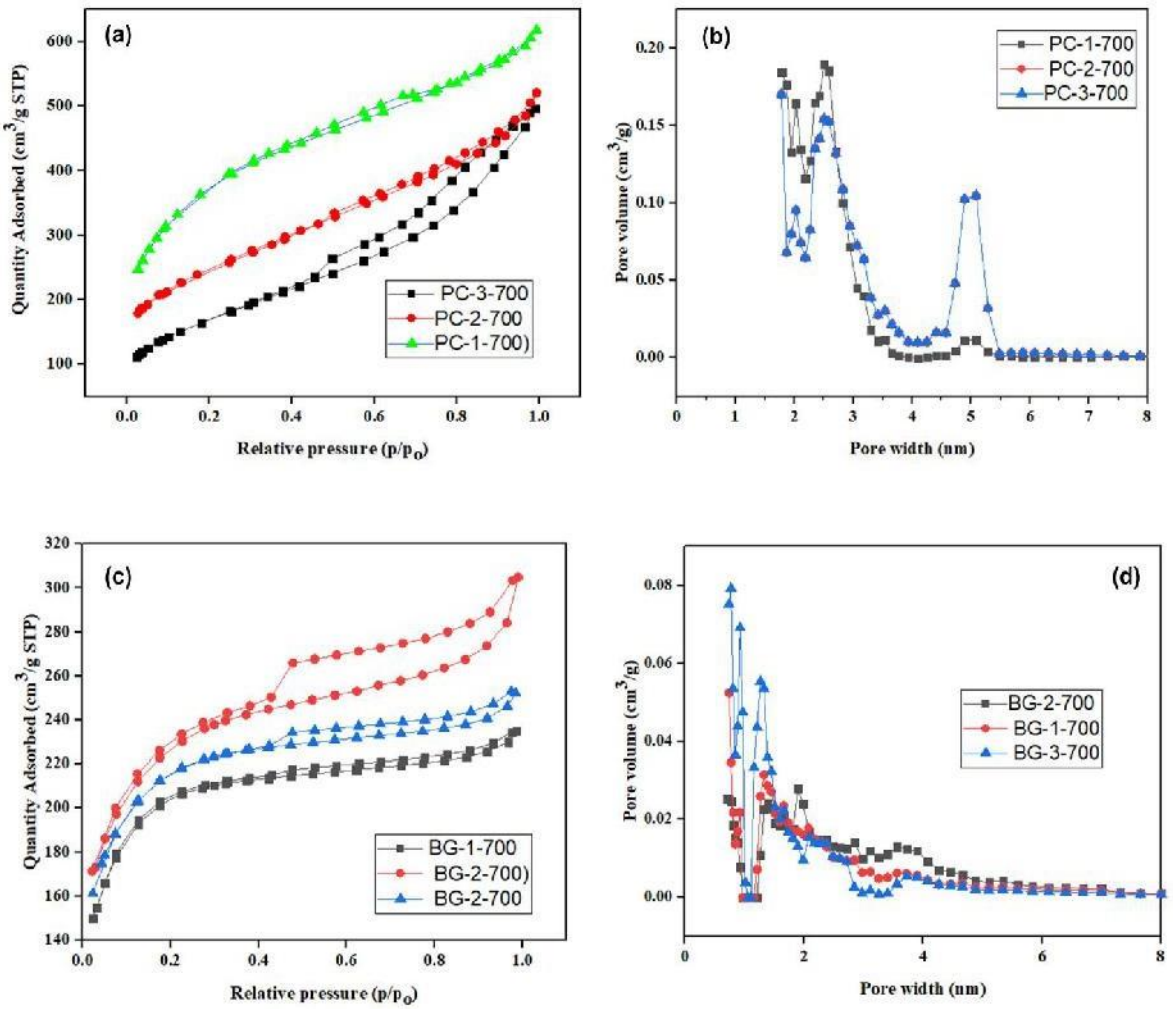


**Figure 8:** **(a) The $N_2$ Adsorption Isotherms for all PC samples (b) The NLDFT pore size distribution for all PC (c) The $N_2$ Adsorption Isotherms for all BG samples (d) The NLDFT pore size distribution for all BG samples**

**Table 3:** **Surface characteristics of all prepared carbon samples**

| Carbon | $S_{BET}$ ($m^2g^{-1}$) | Pore volume ($cm^3g^{-1}$) | Pore size (nm) |
|---|---|---|---|
| BG-1-700 | 576 | 0.7421 | 1.9 |
| BG-2-700 | 927 | 0.6447 | 2.6 |
| BG-3-700 | 830 | 0.5724 | 2.8 |
| PC-1-700 | 454 | 0.7678 | 3.4 |
| PC-2-700 | 549 | 0.709 | 3.3 |
| PC-3-700 | 640 | 0.6071 | 3.1 |

### 4.3 Surface functional group analysis

Figure 9, indicates FTIR analysis of BG and PC samples to confirm the presence of functional groups and chemical bonds. There was no shift in peaks in all prepared samples. In Fig. 9a, peaks about 1394 $cm^{-1}$ are attributed to N-H bending bonds. The Peaks at about 1065 $cm^{-1}$ specify the existence of C-N groups, and peaks at about 712 and 873 $cm^{-1}$ correspond to the bending of the N-H-H bond (Soetemans *et al.*, 2020; Zhang *et al.*, 2019).

A broad absorption peak at around 3062 $cm^{-1}$ is associated with intermolecular stretching of the O-H bond, showing a certain amount of hydroxyl in the carbon. A band at about 1751 $cm^{-1}$ is assigned to a C=O (Sarwar *et al.,* 2021). A characteristic broad peak at 578 $cm^{-1}$ might be located due to the in-plane bending of C-CO-C (Li *et al.,* 2020). For BG samples, notable bands were identified at about 3001 and 2889 $cm^{-1}$, corresponding to the C-H bond's asymmetric and symmetric stretching vibrations (Kyaw *et al.,* 2020). A broad peak at about 2270 and 2080 $cm^{-1}$ corresponds to the presence of CH and CN groups, respectively (Sarwar *et al.,* 2021). The peak at about 1556 $cm^{-1}$ reveals the existence of a CC double bond (Wang *et al.,* 2017). The peak at around 969 $cm^{-1}$ is allocated to the C-O bond. The structure of the $Cd^{2+}$ after electrosorption for the selected electrodes was studied by FTIR analysis, as indicated in Fig. 9 c, d.

Several mechanisms may be involved in $Cd^{2+}$ removal, such as filtration on porous materials, chemisorption including complex compound formation, ion exchange, and electrostatic attraction (Guo *et al.,* 2017; Rao, 2021). As observed in Fig. 9c, there are shifts of peaks, decreases in peak intensity, new peaks formation, and disappearance of peaks, indicating strong interaction between $Cd^{2+}$ ions and the functional groups on the electrode surface. It is noted that the presence of lone pairs of electrons from oxygen functional groups can form complex compounds with $Cd^{2+}$ (Song *et al.,* 2023). Furthermore, according to the hard-soft acid-base theory, nitrogen functional groups in the materials can share electrons for binding with $Cd^{2+}$ , enhancing its removal efficiency (Guo *et al.,* 2017).

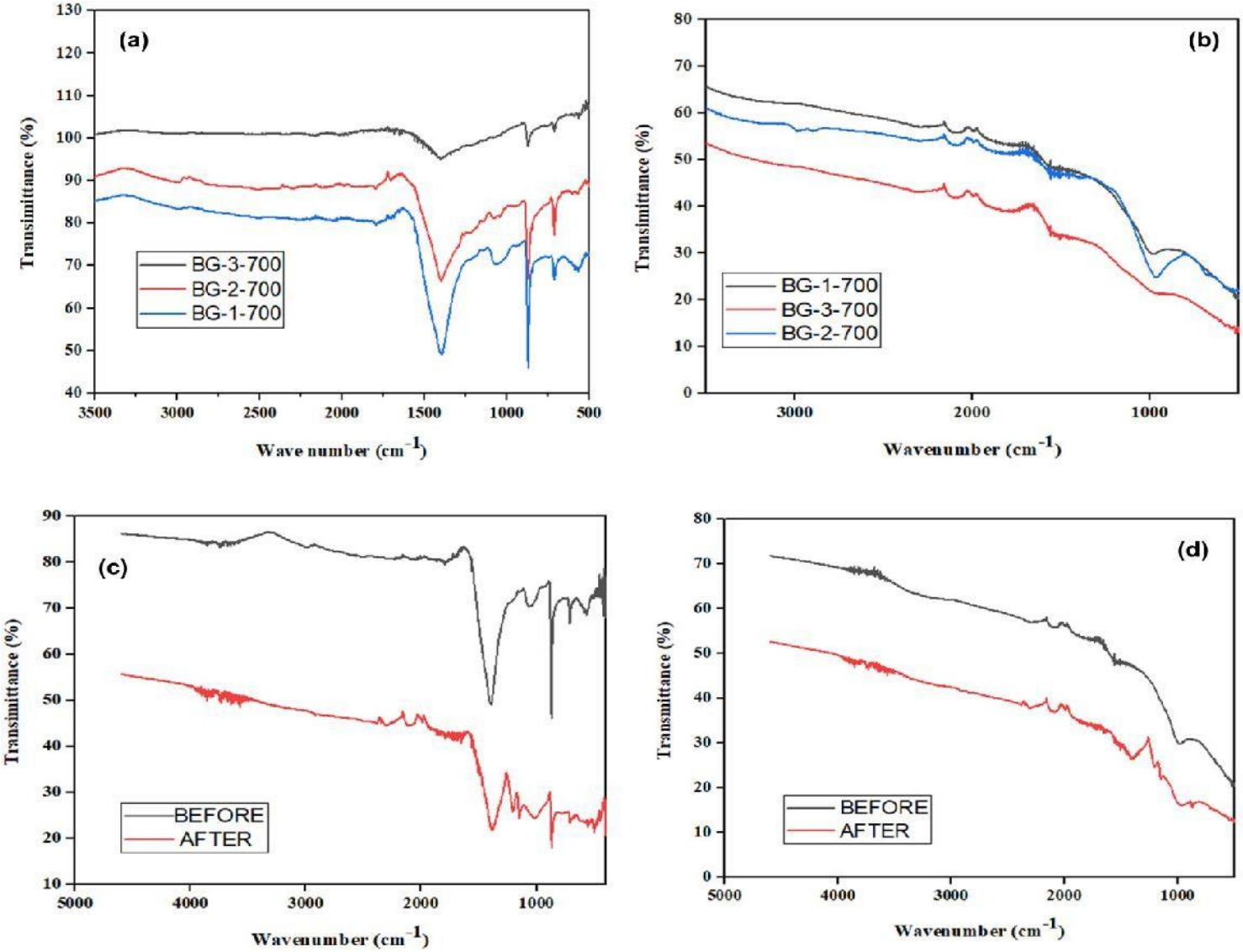


**Figure 9:** **(a) The FTIR spectra for all PC carbon samples (b) The FTIR spectra of PC electrodes before and after $Cd^{2+}$ (c) The FTIR spectra for all BG carbon samples (d) The FTIR spectra of BG electrodes before and after $Cd^{2+}$**

### 4.4 Material crystallinity analysis

Figure 10, shows the x-ray diffraction pattern of selected representatives of PC and BG samples. The diffraction peaks at 25° and 30° are related to the crystal plane of graphite of about (002) and (100), respectively. Broad characteristic peaks reveal the amorphous nature of the prepared PC and BG samples. However, the broadness of the peak in PC samples is more intense, exhibiting a level of crystallinity according to previous results by Purkayastha and Sarkar (2020). Also, there are weak, sharp peaks on the broad peak of BG samples; this may be due to some impurities in the carbon, such as silica, as observed by Enock *et al.* (2017).

The Raman spectroscopy technique of the selected carbon was used to analyze carbon structure, as observed in Fig. 10b. Two peaks were observed at about 1343 and 1586 $cm^{-1}$ in both samples, which are assigned to the existence of D and G bands. Generally, the existence of these bands is shown by the existence of defects in graphitic samples and single graphitic layers, respectively. Hence, the intensity ratio of ($I_D/I_G$) signifies the structural disorder within the material. Therefore, a higher value for PC-2-700 (1.256) than BG-2-700 (0.957) indicated a highly porous structure in PC samples, which may enhance its specific capacitance.

To confirm the existence of Nitrogen content, the XPS analysis was performed on the selected samples, as shown in Fig. 11. The occurrence of peaks at around 398-400.7 eV binding energy evidenced the existence of nitrogen content in prepared carbon. Figure 11a, shows PC and BG carbon O 1s, N 1s, and C 1s from broad spectrum. In Fig. 11e, peaks related to carbon can be observed; C-C/C=C (283.2 eV), C-O (284.59 eV), C=O (285.06 eV), and O-C=O (292.5 eV) for PC carbon (Wang *et al.*, 2018). In Fig. 11d, the peaks for carbon content in BG carbon have a lot of noise, but it shows the presence of carbon. As observed in Fig. 11b, the nitrogen (N 1s peaks) shows the presence of pyrrolic nitrogen (400.7 eV), Amide (399.6 eV), pyridinic nitrogen (398.4 eV) in PC carbon as compared to BG-samples (Enock *et al.*, 2017; Song *et al.*, 2023). The N configurations for PC carbon enhanced the electrosorption capacity of the carbon material such that pyridinic nitrogen may donate one electron pair and increase electron density in the carbon matrix improving electrical conductivity and charge transfer during electrosorption. Also, pyrrolic nitrogen enhances cation affinity by donating lone pairs. Generally, both configurations increase hydrophilicity, improving electrode-electrolyte contact and ion accessibility. In Fig. 11c, the peaks between (530-533 eV) are related to O 1s, whereas C-O is 9530.5 eV.

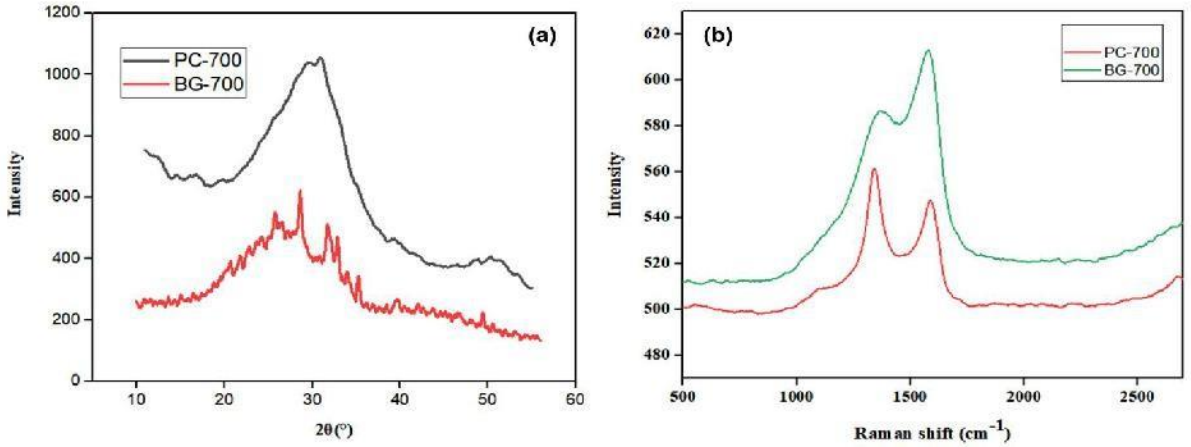


**Figure 10:** **Structural and crystallographic properties of carbon (a) The XRD patterns for PC and BG samples (b) Raman peaks for PC and BG samples**

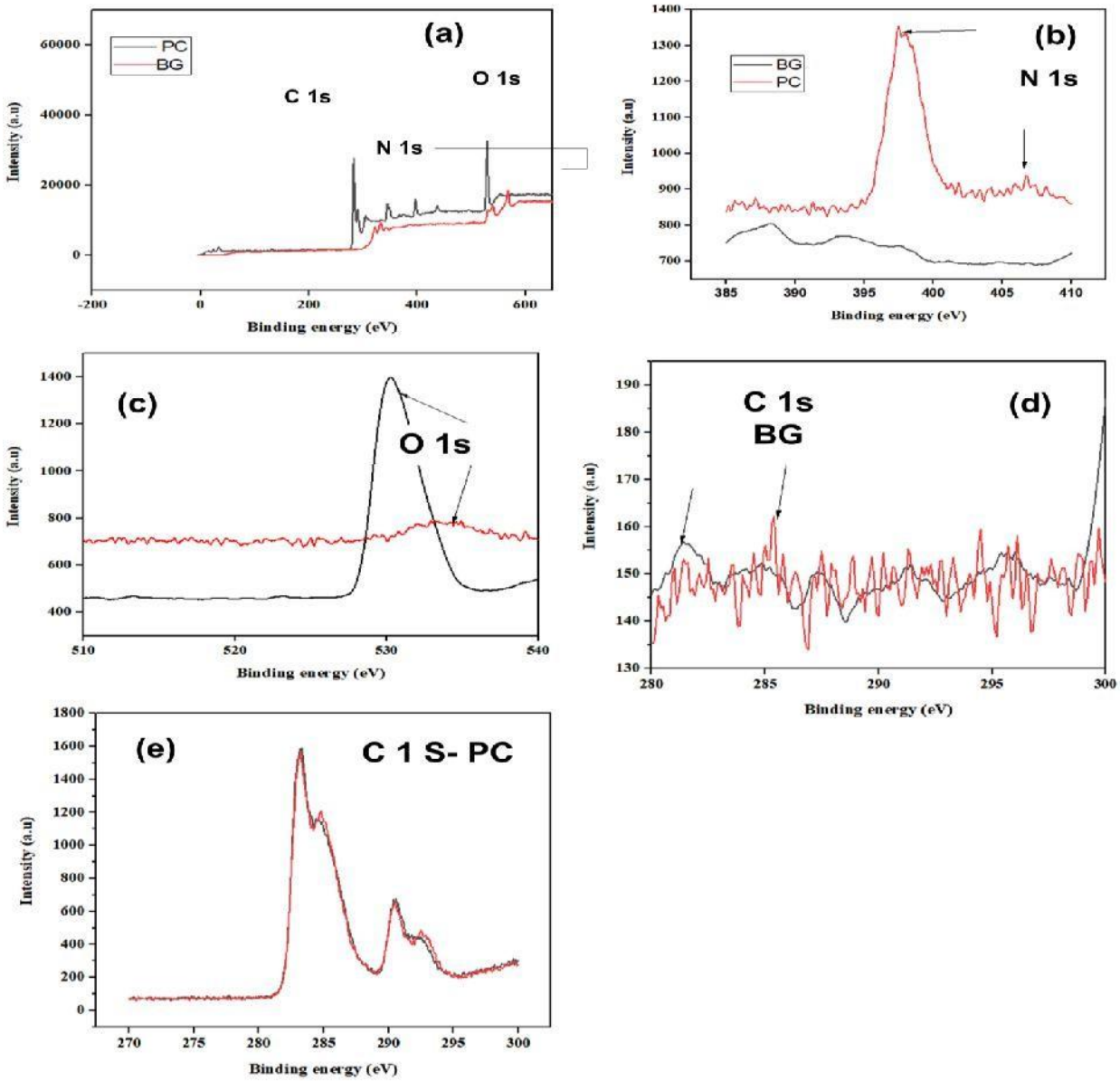


**Figure 11:** **(a) Full spectrum (b) The N 1s spectra (c) The O 1s spectra (d) The C 1s spectra for BG (b) The C 1s spectra for PC**

## 4.5 Electrochemical analysis of the prepared electrodes

Figure 12 and 13, show CV curves of all the prepared electrodes at altered scan rates alternating from 5 to 100 $mVs^{-1}$ in a voltage window of -1.0 V-0.0 V in a 6 M KOH solution. Figure 14, indicate the specific capacitance of all prepared samples concerning scan rate in CV measurement. The CV curves for two materials (PC and BG) exhibited nearly quasi-rectangular shapes at all scan rates, predicting the energy/charge storage mechanism through non-faradaic EDL phenomena. As the scanning rate increases, electrode capacitance decreases, which is always directly related to adsorption capacity. This could be given that high scanning rates prevent ions from having enough time to get along with the materials and penetrate the pores of the materials. Equation 2 was applied to estimate the specific capacitances of pristine PC and BG electrodes. The PC-2-700 electrodes were found to have a better specific capacitance of about 271.9 $Fg^{-1}$ than the BG-2-700 electrodes with (105.8 $Fg^{-1}$). This may be attributed to the good conductivity of PC samples, which results in more active sites for charge storage and transfer availability than BG samples.

However, the overall capacitance of BG samples is low despite its high specific surface area because studies have reported that a large number of micropores hinders the accessibility to electrolyte ions in the solution, hence slowing down the ion transfer to the depth of micropores (Liang *et al.*, 2013; Wang *et al.*, 2019). From Table 4 it can be seen that biomass-derived carbons, including pupae casings (PC) and biogas slurry (BG), exhibit capacitance values comparable to other well-studied biomass electrodes activated under similar conditions. Therefore, they can achieve competitive electrochemical performance, supporting their use as cost-effective and environmentally friendly materials for capacitive deionization and energy storage applications.

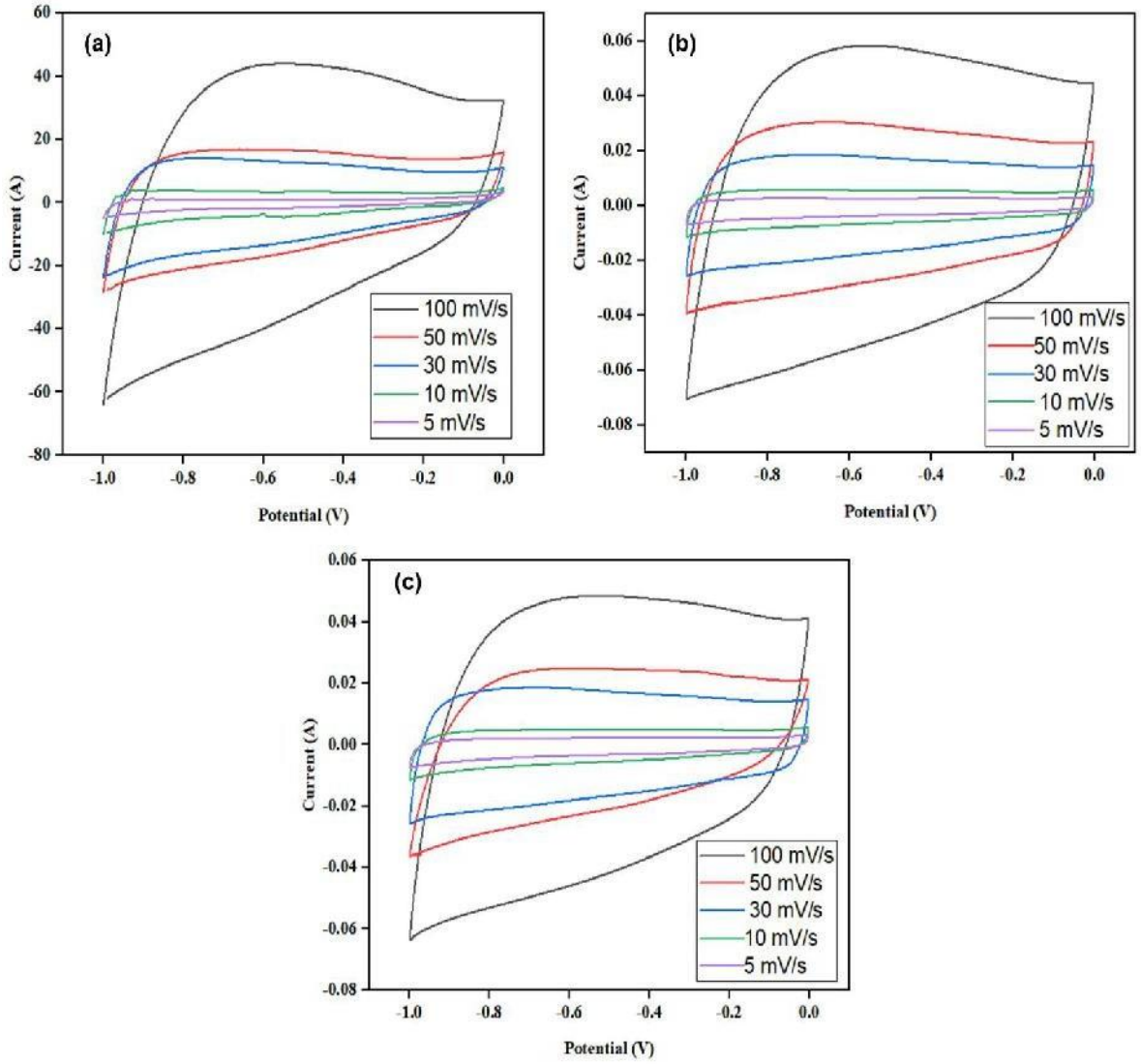


**Figure 12: Cyclic voltammograms (a) The PC-1-700 (b) The PC-2-700, and (c) The PC-3-700**

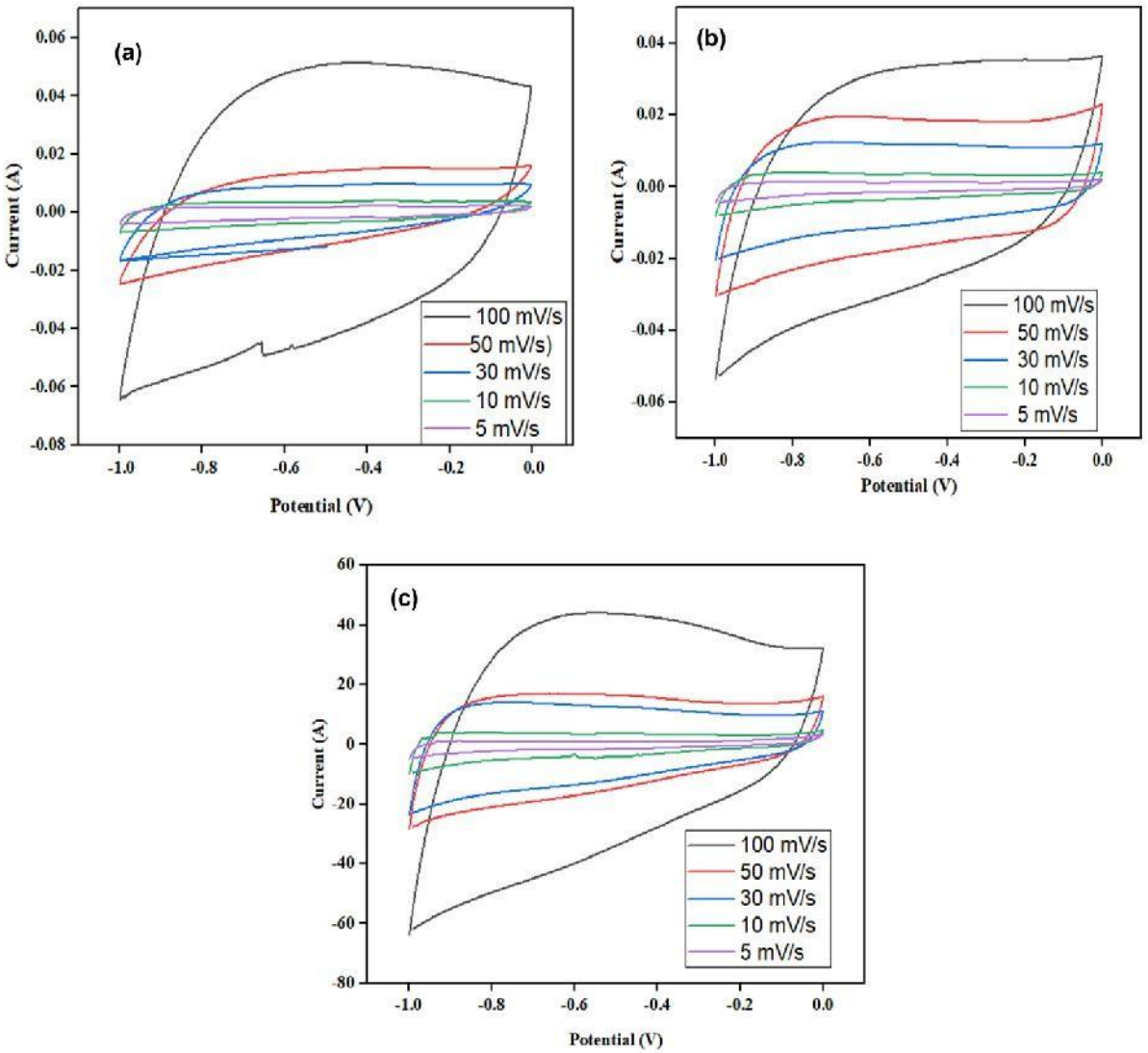


**Figure 13: Cyclic voltammograms (a) The BG-1-700 (b) The BG-2-700, and (c) The BG-3-700**

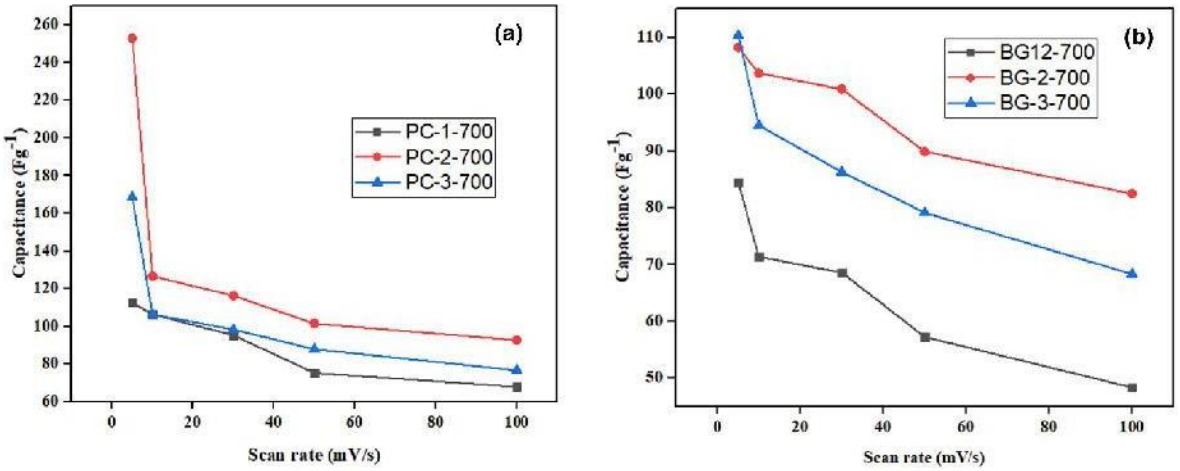


**Figure 14: (a) Specific capacitance of all PC samples concerning scan rate in measurement (b) Specific capacitance of all BG samples concerning scan rate in CV measurement**

**Table 4: Specific capacitance values of activated carbons derived from various biomass feedstocks**

| Biomass waste | Activation temperature (°C ) | Concentration of electrolyte | Capacitance ($Fg^{-1}$) | References |
|---|---|---|---|---|
| Kapok fibers | 750 | 6 M KOH | 283 | Wang *et al.* (2018) |
| Lotus stem | 550 | 6 M KOH | 85 | Yao Zhang *et al.* (2017) |
| Perilla frutescens | 700 | 6 M KOH | 270 | Liu *et al.* (2017) |
| Potato starch | 900 | 1 M KOH | 245 | Ruibin *et al.* (2015) |
| Biogas slurry | 700 | 6 M KOH | 105 | Panja *et al.* (2025) |
| Pupae casings | 700 | 6 M KOH | 271 | Panja *et al.* (2025) |

The EIS test of carbon materials indicates the transfer of charge and ion diffusion at solution/electrode interaction. The EIS spectra for all electrodes are illustrated in Fig. 15. Semi-circle diameter can measure $R_{ct}$ at the point where cadmium chloride solution and electrodes interact. In the low-frequency range, slopes are steeper for PC's electrodes, indicating a higher capacitance and a lower ionic diffusion resistance. Compared to BG electrodes, the semi-circle's diameter was smaller in the high-frequency area, indicating that the material had a high charge transfer rate.

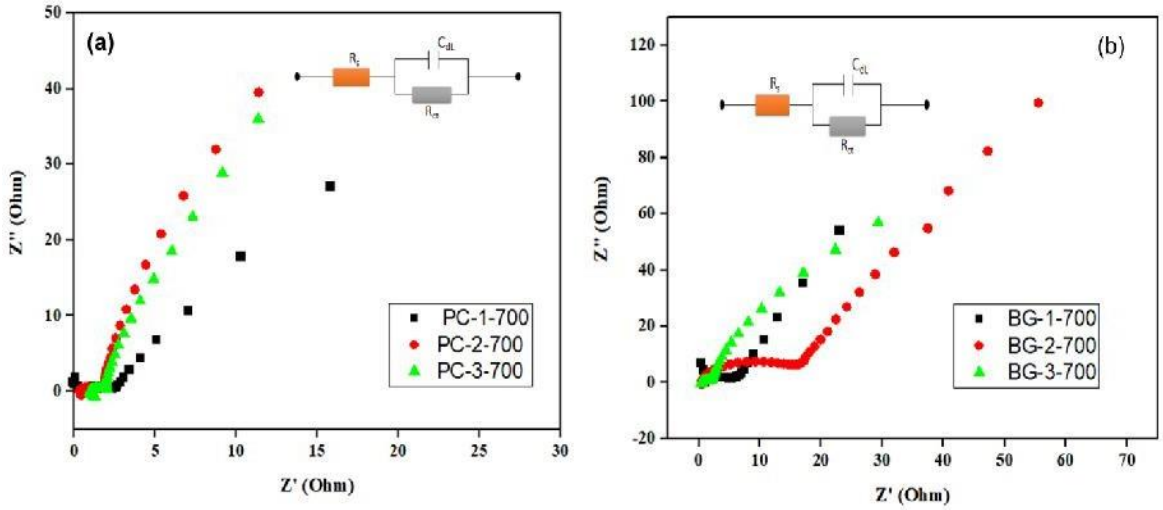


**Figure 15: Nyquist plot (a) All PC samples (b) All BG samples**

The equivalent series resistance (ESR) represents solution resistance ($R_s$), intrinsic active electrode resistance, and contact resistance on electrode/electrolyte interface, which, in theory, is the intercept on the real axis in a high-frequency region (Mo *et al.*, 2016). From the fitted equivalent analogy circuit of the EIS for two selected electrodes, $R_s$ were 0.33 Ω and 0.56 Ω for PC-2-700 and BG-2-700, respectively. However, $R_{ct}$ was 1.03 Ω and 5.57 Ω for PC-2-700 and BG-2-700, respectively, indicating faster ion diffusion onto the surface of the porous PC-2-700 electrode than on BG-2-700. The larger $R_{ct}$ value for BG-2-700 may be due to many small micropores and less hydrophilic nature, resulting in poor $Cd^{2+}$ removal efficiency (Wang

*et al.*, 2018). Table 5 illustrates $R_s$ and $R_{ct}$ for all prepared electrodes. Generally, the KOH activation of PC-2-700 improves the electrochemical properties of the PC-2-700, resulting in fast charge transfer and better electric conductivity, significantly enhancing the electrosorption ability in the CDI test.

**Table 5: The Rs and Rct value obtained from fitted equivalent circuit for the electrodes**

| SAMPLE | $R_s(\Omega)$ | $R_{ct}$ ($\Omega$) |
|---|---|---|
| PC-1-700 | 0.45 | 2.51 |
| PC-2-700 | 0.33 | 1.03 |
| PC-3-700 | 0.35 | 1.96 |
| BG-1-700 | 0.71 | 10.98 |
| BG-2-700 | 0.56 | 5.57 |
| BG-3-700 | 0.62 | 7.68 |

### 4.6 Wettability measurement

The wettability properties of the selected carbons for both PC and BG carbons are shown in Fig. 16. The images were captured at three-second intervals. At instant capture, the contact angles were 79° and 138.67° for PC and BG carbons, respectively. It reaches 18.66° and 71.49° after 12 sec, respectively. This indicates that PC carbons are more hydrophilic than BG carbons, which will enhance their adsorption and electrosorption ability. These properties facilitate the high use of pores on the surface of PC carbons, which also increases the electrode/solution interaction and eventually enhances the adsorption of $Cd^{2+}$ (Zhao *et al.*, 2023). Nitrogen functional groups enhanced this finding in addition to –CO and –OH groups on the PC carbon surface, as observed in the FTIR peaks. The low level of hydrophilicity in BG carbon, despite the presence of some N/O groups may be attributed to their placement inside the micropores and may not contribute to electrosorption if pores were inaccessible.

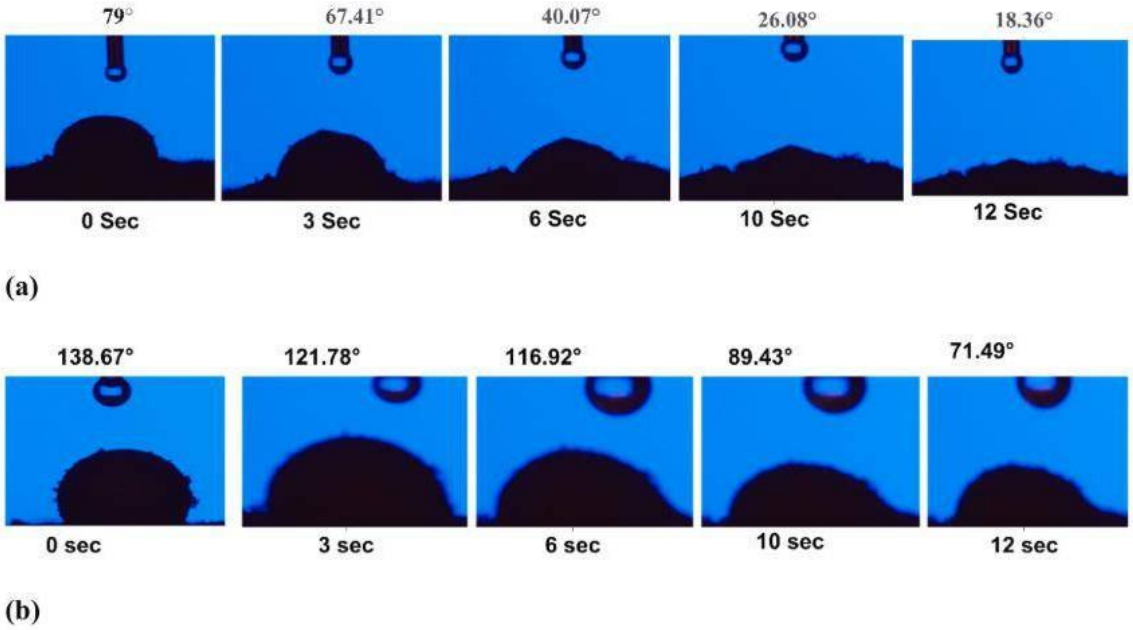


**Figure 16: Photographs of water drops (a) The PC sample and (b) The BG sample**

### 4.7 The CDI experiment

The CDI performance of the PC and BG electrodes in removing $Cd^{2+}$ from water was investigated in this work. The concentration of $Cd^{2+}$ ions before and after the electrosorption process was estimated by Atomic Absorption spectrometry. The solution containing 5 and 10 $mgL^{-1}$ of $Cd^{2+}$ as the initial concentration was prepared with a pH above 9. At this pH, $Cd(OH)_2$ is formed, which tends to aggregate at the surface of the working electrodes, contributing to the removal of $Cd^{2+}$ from water (Song *et al.*, 2023). The conductivity drop of the prepared solution (5 mg/L and 10 mg/L) versus time within 90 min electrosorption at 1.2 V was used to predict the concentration drop as presented in Fig. 17b and 18b. Concentration dropped to 0.45 $mgl^{-1}$ and 2.01 $mgl^{-1}$ for PC-2-700 and BG-3-700, reaching an efficiency of 91% and 60%, respectively, at 5 $mgL^{-1}$ of $Cd^{2+}$ (Table 6). An observation of a decrease in conductivity for all electrodes is seen, and within less than 90 min, materials reach saturation point. As can be seen in Fig. 18a and 17a, conductivity dropped from 398 $\mu Scm^{-1}$ to 87 $\mu Scm^{-1}$ and 395 $\mu Scm^{-1}$ to 213.3 $\mu Scm^{-1}$ during the electrosorption process for PC-2-700 and BG-2-700 electrodes at 5 mg/L concentration, respectively.

Equation 1 was used to estimate the electrodes' electrosorption capacity. The PC-2-700 exhibited the highest electrosorption capacity, approximately 10.9 and 11.2 $mgg^{-1}$, at 5 and 10 $mgg^{-1}$ concentrations, respectively. This result corresponds with its highest removal for $Cd^{2+}$ ions, as discussed in the electrosorption process.

Cycling stability and regeneration ability are essential when choosing a better CDI electrode material. A direct short-circuit regeneration of 23 electrosorption/desorption cycles for 12 hours was done in a 5 mg/L $CdCl_2$ solution at 1.2 V for the selected electrode. Figure 18c, shows that the pupae casings-derived electrode demonstrated good cyclic stability in CDI, retaining over 89.7% of its initial $Cd^{2+}$ removal efficiency after regeneration. An increase in conductivity was observed when the negative and positive plates were shorted-off, revealing that desorption took place. This may be attributed to the complex compound between $Cd^{2+}$ and hydroxyl groups existing on the material's surface, which may affect its regeneration (Song *et al.*, 2023). This shows that the carbon surface morphology may affect the electrode materials' removal efficiency and regeneration. As indicated in Fig. 17b and 18b, the electrode removal efficiency decreases when the concentration of $Cd^{2+}$ increases to 10 $mgl^{-1}$. While increasing the concentration of $Cd^{2+}$ in the solution to 10 $mgl^{-1}$, the removal efficiency decreases to 48, 61, and 52% for PC-1-700, PC-2-700, and PC-3-700, respectively, and to 20, 30, and 33% for BG-1-700, BG-2-700, and BG-3-700, respectively.

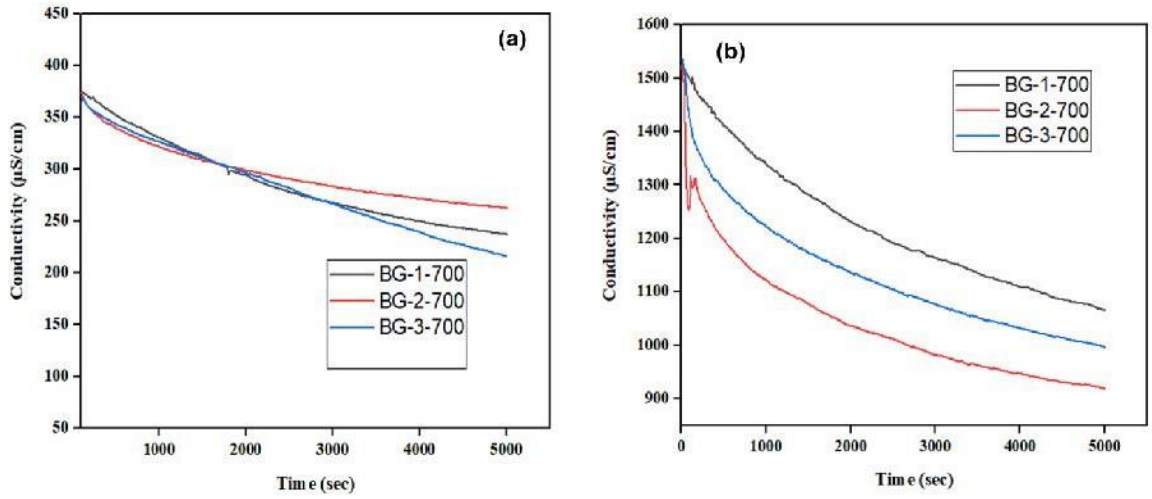


**Figure 17: (a) Desalination experiment of all BG samples at 5 mg/L (b) at 10 mg/L**

The electrosorption capacity for PC-2-700 increases to 11.2 $mgg^{-1}$, as shown in Table 6. This indicates the promising application of PC-based electrodes in recovering $Cd^{2+}$ from aqueous solutions.

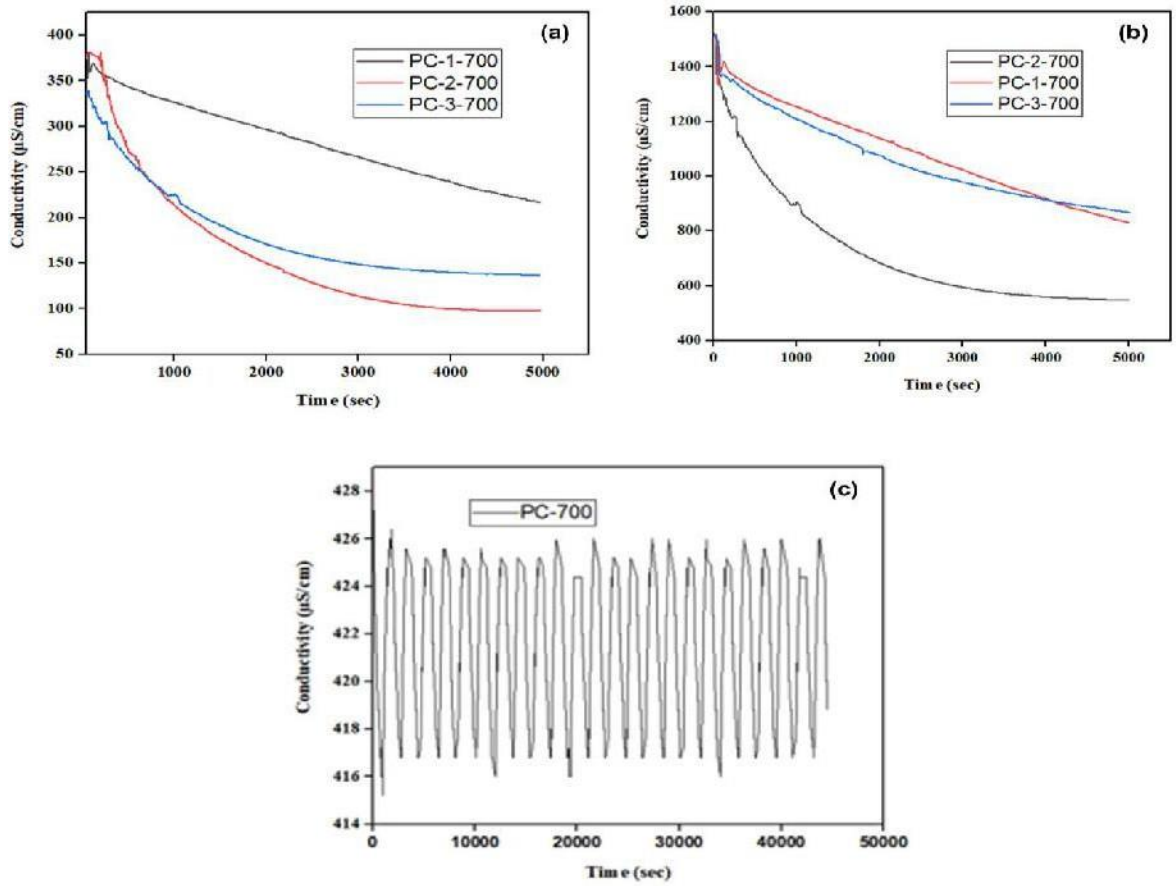


**Figure 18: Desalination experiment of all PC samples at 5 mg/L (b) at 10 mg/L (c) Regeneration cycles for PC electrode**

**Table 6: The $Cd^{2+}$ Removal efficiency determined by AAS measurement**

| Samples | AAS Initial concentration (mg/L) | AAS Final concentration (mg/L) | Removal efficiency (%) | Electroporation Capacity($mgg^{-1}$) |
|---|---|---|---|---|
| PC-1-700 | 5 | 1.7512 | 65 | 5.2 |
| | 10 | 5.2110 | 48 | 3.1 |
| PC-2-700 | 5 | 0.4532 | 91 | 10.9 |
| | 10 | 3.9121 | 61 | 11.2 |
| PC-3-700 | 5 | 1.0113 | 80 | 8.3 |
| | 10 | 4.7782 | 52 | 5.4 |
| BG-1-700 | 5 | 3.1513 | 37 | 1.2 |
| | 10 | 8.1435 | 20 | 0.3 |
| BG-2-700 | 5 | 2.0134 | 56 | 2.1 |
| | 10 | 7.2113 | 30 | 1.6 |
| BG-3-700 | 5 | 2.0023 | 60 | 2.3 |
| | 10 | 6.7121 | 33 | 0.6 |

Table 7 provides an overview of recent CDI electrode materials reported in a research paper for removing Cadmium ions from water. The activated carbon (AC) cloth's $Cd^{2+}$ reduction efficiency was 41.87% (Huang *et al.*, 2016); when birnessite electrodes were used, the

electrosorption capacity was about 54.78 $mgg^{-1}$ (Peng *et al.*, 2016). Also, the Activated carbon fiber/$Mno_2$-based electrode was investigated for $Cd^{2+}$ removal, and the electrosorption capacity reached 14.88 $mgg^{-1}$ (Yin *et al.*, 2022). Polypyrrole/chitosan composite-based electrode was used for $Cd^{2+}$ removal, and the removal efficiency was 51.10% (Zhang *et al.*, 2019). The AC from 3 biomasses was investigated for recovering $Cd^{2+}$ from water (Song *et al.*, 2023).

Therefore, electrode materials prepared from environmentally friendly and low-cost black soldier fly pupae casings and biogas slurry exhibited similar efficiency of capacitive deionisation in removing cadmium from water.

**Table 7: Materials used in CDI to remove cadmium ions from water**

| Materials | $RE$ % | EC (mg/g) | Initial concentration ($mgL^{-1}$) | V(v) | Time (h) | Volume (ml) | Flow rate (ml/min) | Approach | Specific surface area ($m^2g^{-1}$) | References |
|---|---|---|---|---|---|---|---|---|---|---|
| Activated carbon cloth | 32 | 103.6 | - | 1.2 | - | - | 0 | Batch mode | - | Huang *et al.* (2016) |
| Activated carbon cloth with ZnO nanoparticles | 29 | - | 50 | 1.8 | - | 3.2 | 3 | Batch mode | 1000 | Kyaw *et al.* (2020) |
| Birnessite-activated electrodes | - | 900 | 200 | - | 2 | - | - | Batch mode | 14.2 | Peng *et al.* (2016) |
| Armophous O-doped boron nitride nanosheets | - | 2281 | - | - | - | 12.5 | - | - | - | Chen *et al.* (2017) |
| Lotus leaf-derived carbon nanosheets | 71 | - | 100 | 1.2 | - | - | | - | 3705 | Ye *et al.* (2025) |
| Nitrogen doped porous carbon material | 82 | - | 10 | 1.2 | - | - | - | - | 798 | Wang *et al.* (2024) |
| N-doped Biochar Humic acid. | 89 | 79 | 4 | 1.2 | 2 | - | - | Batch mode | - | Lin *et al.* (2022) |
| $MoS_2$/AC nanosheet composite. | 58.06 | 22.15 | 0.001 | - | - | - | - | Batch mode | - | Yin *et al.* (2022) |
| Pamello peel | 73<br>52 | 1.6<br>7 | 2<br>10 | 1.2 | - | - | - | - | | Song *et al.* (2023) |

| Materials | $RE$ % | EC (mg/g) | Initial concentration ($mgL^{-1}$) | V(v) | Time (h) | Volume (ml) | Flow rate (ml/min) | Approach | Specific surface area ($m^2g^{-1}$) | References |
|---|---|---|---|---|---|---|---|---|---|---|
| Algae | 89 | 2.1 | 2 | 1.2 | - | - | - | - | | Panja *et al.* (2025) |
| | 73 | 8.6 | 10 | | | | | | | |
| Corncob | 89 | 2.1 | 2 | 1.2 | | | | | | |
| | 76 | 9.1 | 10 | | | | | | | |
| Pupae casings | 91 | 10.9 | 5 | | | | | | 546 | |
| | 61 | 11.2 | 10 | 1.2 | 1.5 | 30 | | Batch mode | | |
| Biogas slurry | 46 | 4.4 | 5 | | | | | | 927 | |
| | 30 | 1.6 | 10 | | | | | | | |

Table 8 summarizes how the variation of the activation agent ratio affects the characteristics of the prepared samples. The data indicates a direct relationship between the ratio of the activation agent and the BET area of the sample. Specifically, as the amount of KOH increases, the surface area also increases. This is because adding more KOH during the activation process expands the existing pores, thereby increasing surface area and pore volume, as observed by Enock *et al.* (2017). However, the sorption capacity decreases despite the larger surface area associated with large KOH ratios. This suggests that surface area alone does not guarantee superior electrosorption performance in CDI applications. The effectiveness of electrosorption is also influenced by factors such as the availability of active sites and electric double-layer overlap. A balance concerning these electrosorption sites and EDL overlap is crucial to achieving optimal electrosorption capacity. Additionally, the performance in CDI is enhanced by the pore structure and size of the electrodes; better ion adsorption occurs when the pore size is compatible with the hydrated ion size. A well-balanced distribution of micropores and mesopores is also essential for improving removal efficiency as noted by Wang *et al.* (2024).

**Table 8: Relationship between the prepared samples' textural properties and effects of activation**

| Carbon | $S_{BET}$ ($m^2 g^{-1}$) | Pore volume ($cm^3 g^{-1}$) | Pore size (nm) |
|---|---|---|---|
| BG-1-700 | 576 | 0.5421 | 1.9 |
| BG-2-700 | 927 | 0.6447 | 2.6 |
| BG-3-700 | 830 | 0.5724 | 2.8 |
| PC-1-700 | 454 | 0.7678 | 3.4 |
| PC-2-700 | 549 | 0.709 | 3.3 |
| PC-3-700 | 640 | 0.5071 | 3.1 |

# CHAPTER FIVE

# CONCLUSION AND RECOMMENDATIONS

## 5.1 Conclusion

This work explored the development and application of porous carbon derived from biogas slurry, and black soldier fly pupae casings for removing cadmium ions from water with an energy-efficient capacitive deionization technique. The study involved the preparation of pupae casings and biogas slurry-derived carbons through carbonization and activation with potassium hydroxide. The structural and chemical properties and differences in the activation agent-to-pupae casings/biogas slurry ratio at fixed activation temperatures were examined from various characterization analyses such as SEM-EDS, BET, FTIR, XPS, XRD, Raman spectroscopy, and electrochemical test. The surface and structural analysis showed a well- formed pore and mesopores dominance for PC- carbon as compared to BG carbon with high microporosity which limits ions accessibility, hence lowering its capacitance and electrosorption capacity.

The electrochemical and textural analysis results revealed a high structural disorder (amorphous) for PC carbon, enhancing capacitance and better wettability than BG- carbon. This study assessed the usefulness of these carbon electrodes in removing Cadmium ions ($Cd^{2+}$) from aqueous solutions.

The results showed that PC-2-700 has a high removal efficiency of about 91% with a 10.9 electrosorption capacity. A material with high SSA (927 $m^2/g$ for BG-2-700) has a moderate $Cd^{2+}$ removal of about 56%. The results did not reveal a direct correlation between the KOH-to-carbon ratio and the efficiency of $Cd^{2+}$ removal. However, even if BET surface area is a significant factor, it is not the single determinant of electrosorption capacity and removal effectiveness. This is because high surface area does not guarantee that all pores were accessible during removal process.

The existence of nitrogen content in carbon materials may significantly enhance material's electrochemical activity and ion affinity, improving removal efficiency beyond what surface areas alone can provide (Xu *et al.*, 2023; Zhang *et al.*, 2019). The study demonstrates that pupae casing-derived activated carbon is a promising low-cost, sustainable solution for cadmium

removal, potentially supporting rural water purification strategies and circular economy principles.

## 5.2 Recommendations

This study recommends several areas for further investigation:

(i) Optimization of parameters: Although the synthesis of PC and BG-derived carbon materials for CDI applications has shown promising results, further optimization of the carbonization and activation temperatures is necessary to understand the suitable parameters for good carbon for better performance in CDI and pH and voltage.

(ii) Metal oxide hybrid: While this study focused on pristine carbon, future research should consider integrating redox-active oxide into carbon matrix to improve ion affinity.

(iii) Broader water purification testing: The synthesized porous carbons should be evaluated for their effectiveness in removing other contaminants from water, including fluoride, salts, and additional heavy metals, to assess their broader applicability in water purification.

(iv) Competitive ion study: Future study should consider removing the cadmium ion in the presence of competing ions ($Pb^{2+}$, $Cr^{2+}$, $Na^{+}$) to access ion selectivity.

By addressing these recommendations, future research can build upon the findings of this study and potentially enhance the practical applications of black soldier pupae casings and biogas slurry-derived carbon in environmental remediation.

## REFERENCES


Akl, M., Dawy, M. B., & Serage, A. A. (2014). Efficient removal of phenol from water samples using sugarcane bagasse based activated carbon. *Journal of Analytical and Bioanalytical Techniques, 5*(2), 1-12.

Alfredy, T., Jande, Y., & Pogrebnaya, T. (2019). Removal of lead ions from water by capacitive deionization electrode materials derived from chicken feathers. *Journal of Water Reuse and Desalination*, *9*(3), 282-291.

Ali, M. M., Ali, M. L., Islam, M. S., & Rahman, M. Z. (2016). Preliminary assessment of heavy metals in water and sediment of Karnaphuli River, Bangladesh. *Environmental Nanotechnology, Monitoring & Management*, *5*, 27-35.

Alvizuri-Tintaya, P. A., Villena-Martínez, E. M., Lo-Iacono-Ferreira, V. G., Torregrosa-López, J. I., Lora-García, J., & D'Abzac, P. (2023). Mathematical and Statistical Evaluation of Reverse Osmosis in the Removal of Manganese as a Way to Achieve Sustainable Operating Parameters. *Membranes*, *13*(8), 724.

Bandara, T., Xu, J., Potter, I. D., Franks, A., Chathurika, J., & Tang, C. (2020). Mechanisms for the removal of Cd (II) and Cu (II) from aqueous solution and mine water by biochars derived from agricultural wastes. *Chemosphere*, *254*, 126745.

Chen, M. M., Wei, D., Chu, W., Wang, T., & Tong, D. G. (2017). Retracted Article: One-pot synthesis of O-doped BN nanosheets as a capacitive deionization electrode for efficient removal of heavy metal ions from water. *Journal of Materials Chemistry A*, *5*(32), 17029-17039. https://doi.org/10.1039/C7TA05459A

Chen, R., Sheehan, T., Ng, J. L., Brucks, M., & Su, X. (2020). Capacitive deionization and electrosorption for heavy metal removal. *Environmental Science: Water Research & Technology*, *6*(2), 258-282.

Chen, Y., Zhang, G., Zhang, J., Guo, H., Feng, X., & Chen, Y. (2018). Synthesis of porous carbon spheres derived from lignin through a facile method for high performance supercapacitors. *Journal of Materials Science & Technology*, *34*(11), 2189-2196.

Choirul, M., Nurhadi, M., Kusumawardani, R., Anisa, S., Yulian, S. A., Rahma, S. A., Akbar, M., Umar, A. H., Guo, Y., & Lai, S. Y. (2024). Carbon-derived Black Soldier Fly Larvae for Adsorption of Methylene Blue Dye: Characterization, Kinetic and Thermodynamic Studies. *Malaysian Journal of Fundamental and Applied Sciences*, *20*(1), 191-202.

Chowdhury, S., Mazumder, M. J., Al-Attas, O., & Husain, T. (2016). Heavy metals in drinking water: Occurrences, implications, and future needs in developing countries. *Science of the Total Environment*, *569*, 476-488.

Deng, Z., Sun, S., Li, H., Pan, D., Patil, R. R., Guo, Z., & Seok, I. (2021). Modification of coconut shell-based activated carbon and purification of wastewater. *Advanced Composites and Hybrid Materials*, *4*, 65-73.

Edokpayi, J. N., Odiyo, J. O., & Olasoji, S. O. (2014). Assessment of heavy metal contamination of Dzindi river, in Limpopo Province, South Africa. *International Journal of Natural Science Research*, *2*(10), 185-194.

Elisadiki, J., Jande, Y. A. C., Kibona, T. E., & Machunda, R. L. (2020). Highly porous biomass-based capacitive deionization electrodes for water defluoridation. *Ionics*, *26*(5), 2477-2492.

Elisadiki, J., Jande, Y. A. C., Machunda, R. L., & Kibona, T. E. (2019). Porous carbon derived from Artocarpus heterophyllus peels for capacitive deionization electrodes. *Carbon*, *147*, 582-593.

Enock, T. K., King'ondu, C. K., Pogrebnoi, A., & Jande, Y. A. C. (2017). Biogas-slurry derived mesoporous carbon for supercapacitor applications. *Materials Today Energy*, *5*, 126-137.

Farma, R., Julita, R. I., Apriyani, I., Awitdrus, A., & Taer, E. (2023). $ZnCl_2$*-Assisted Synthesis of Coffee Bean Bagasse-Based Activated Carbon as a Stable Material for High-Performance Supercapacitors*. https://scholar.google.com

Gaikwad, M. S., & Balomajumder, C. (2017). Tea waste biomass activated carbon electrode for simultaneous removal of Cr (VI) and fluoride by capacitive deionization. *Chemosphere*, *184*, 1141-1149.

Gao, M., Li, J., Wang, Z., Yang, Z., Chen, Y., Deng, W., Liang, W., Ao, T., & Chen, W. (2024). Hierarchical nickel cobaltite nanoneedle arrays armored flexible electrospinning carbon

nanofibers membrane for electrochemical deionization. *Separation and Purification Technology*, *328*, 125084. https://doi.org/https://doi.org/10.1016/j.seppur.2023.125084

Gong, W., Yang, Y., Chang, H., Wang, T., & Liang, H. (2022). Evaluating the performance of flow-electrode capacitive deionization for cadmium removal from aqueous solution. *Journal of Water Process Engineering*, *46*, 102595.

Guo, Z., Zhang, X., Kang, Y., & Zhang, J. (2017). Biomass-Derived Carbon Sorbents for Cd(II) Removal: Activation and Adsorption Mechanism. *ACS Sustainable Chemistry & Engineering*, *5*(5), 4103-4109. https://doi.org/10.1021/acssuschemeng.7b00061

He, G., Yan, G., Song, Y., & Wang, L. (2020). Biomass juncus derived nitrogen-doped porous carbon materials for supercapacitor and oxygen reduction reaction. *Frontiers in Chemistry*, *8*, 226.

Hsu, C. C., Tu, Y. H., Yang, Y. H., Wang, J. A., & Hu, C. C. (2020). Improved performance and long-term stability of activated carbon doped with nitrogen for capacitive deionization. *Desalination*, *481*, 114362.

Huang, Z., Lu, L., Cai, Z., & Ren, Z. J. (2016). Individual and competitive removal of heavy metals using capacitive deionization. *Journal of Hazardous Materials*, *302*, 323-331. https://doi.org/https://doi.org/10.1016/j.jhazmat.2015.09.064

Jande, Y. A. C. (2015). *Modeling and Application of Capacitive Deionization in Desalination and $CO_2$ capture*. https://scholar.google.com

Kacholi, D. S., & Sahu, M. (2018). Levels and health risk assessment of heavy metals in soil, water, and vegetables of Dar es Salaam, Tanzania. *Journal of Chemistry*, *2018*, 1-9.

Kassenga, G. R., & Mbuligwe, S. E. (2009). Impacts of a solid waste disposal site on soil, surface water and groundwater quality in Dar es Salaam City, Tanzania. *Journal of Sustainable Development in Africa*, *10*(4), 73-94.

Kaya, M., Sofi, K., Sargin, I., & Mujtaba, M. (2016). Changes in physicochemical properties of chitin at developmental stages (larvae, pupa and adult) of Vespa crabro (wasp). *Carbohydrate Polymers*, *145*, 64-70.

Khan, S. A., Malav, L., Kumar, S., Malav, M., & Gupta, N. (2014). Resource utilization of biogas slurry for better yield and nutritional quality of baby corn. *Advances in Environmental and Agricultural Science*, *32*, 382-394.

Kim, M., Lim, H., Xu, X., Hossain, M. S. A., Na, J., Awaludin, N. N., Shah, J., Shrestha, L. K., Ariga, K., Nanjundan, A. K., & Martin, D. J. (2021). Sorghum biomass-derived porous carbon electrodes for capacitive deionization and energy storage. *Microporous and Mesoporous Materials*, *312*, 110757.

Kyaw, H. H., Myint, M. T. Z., Al-Harthi, S., & Al-Abri, M. (2020). Removal of heavy metal ions by capacitive deionization: Effect of surface modification on ions adsorption. *Journal of Hazardous Materials*, *385*, 121565.

Lado, J. J., Zornitta, R. L., Calvi, F. A., Tejedor-Tejedor, M. I., Anderson, M. A., & Ruotolo, L. A. (2016). Study of sugar cane bagasse fly ash as electrode material for capacitive deionization. *Journal of Analytical and Applied Pyrolysis*, *120*, 389-398.

Li, P., Feng, T., Song, Z., Tan, Y., & Luo, W. (2020). Chitin derived biochar for efficient capacitive deionization performance. *RSC Advances*, *10*(50), 30077-30086.

Liang, Y., Liang, F., Zhong, H., Li, Z., Fu, R., & Wu, D. (2013). An advanced carbonaceous porous network for high-performance organic electrolyte supercapacitors. *Journal of Materials Chemistry A*, *1*(24), 7000-7005.

Lin, S., Yang, X., Liu, L., Li, A., & Qiu, G. (2022). Electrosorption of cadmium and arsenic from wastewaters using nitrogen-doped biochar: Mechanism and application. *Journal of Environmental Management*, *301*, 113921.

Liu, B., Liu, Y., Chen, H., Yang, M., & Li, H. (2017). Oxygen and nitrogen co-doped porous carbon nanosheets derived from Perilla frutescens for high volumetric performance supercapacitors. *Journal of Power Sources*, *341*, 309-317.

Liu, D., Zhang, W., Lin, H., Li, Y., Lu, H., & Wang, Y. (2016). A green technology for the preparation of high capacitance rice husk-based activated carbon. *Journal of Cleaner Production*, *112*, 1190-1198.

Lumami, K. V., García-Alvarez, M., Sang-Sefidi, V., Buleng, N. T. E., Ndikumana, T., Musibono, D. D., Van-der-Bruggen, B., & Luis, P. (2022). Evaluation of commercial

reverse osmosis and nanofiltration membranes for the removal of heavy metals from surface water in the Democratic Republic of Congo. *Clean Technologies*, *4*(4), 1300-1316.

Lwimbo, Z. D., Komakech, H. C., & Muzuka, A. N. (2019). Impacts of emerging agricultural practices on groundwater quality in Kahe catchment, Tanzania. *Water*, *11*(11), 2263.

Ma, J., Li, S. L., Chen, Y., Yue, F. J., Shaheen, S. M., Majrashi, A., Ali, E. F., Antoniadis, V., Rinklebe, J., Luo, H., & Zheng, Q. (2022). Hazardous toxic metal (loid) s in top-and deep-soils during the transformation of aquaculture ponds restored to farmland. *Science of the Total Environment*, *852*, 158569.

Machunda, R., Jeon, H., Lee, J., & Lee, J. (2009). Effects of acid treatment on the improvement of specific capacitance and deionization efficiency of porous carbon electrodes. *Water Science and Technology: Water Supply*, *9*(2), 159-165.

Maftouh, A., El-Fatni, O., El-Hajjaji, S., Jawish, M. W., & Sillanpää, M. (2023). Comparative review of different adsorption techniques used in heavy metals removal in water. *Biointerface Research in Applied Chemistry*, *13*, 397.

Martínez, J. P., Falomir, M. P., & Gozalbo, D. (2014). *Chitin: A Structural Biopolysaccharide with Multiple Applications*. https://scholar.google.com

Mawari, G., Kumar, N., Sarkar, S., Frank, A. L., Daga, M. K., Singh, M. M., Joshi, T. K., & Singh, I. (2022). Human health risk assessment due to heavy metals in ground and surface water and association of diseases with drinking water sources: A study from Maharashtra, India. *Environmental Health Insights*, *16*, 11786302221146020.

Mdegela, R., Braathen, M., Pereka, A., Mosha, R., Sandvik, M., & Skaare, J. (2009). Heavy metals and organochlorine residues in water, sediments, and fish in aquatic ecosystems in urban and peri-urban areas in Tanzania. *Water, Air, and Soil Pollution*, *203*, 369-379.

Mo, R. J., Zhao, Y., Wu, M., Xiao, H. M., Kuga, S., Huang, Y., Li, J. P., & Fu, S. Y. (2016). Activated carbon from nitrogen rich watermelon rind for high-performance supercapacitors. *RSC Advances*, *6*(64), 59333-59342.

Mohammadi, A. A., Zarei, A., Majidi, S., Ghaderpoury, A., Hashempour, Y., Saghi, M. H., Alinejad, A., Yousefi, M., Hosseingholizadeh, N., & Ghaderpoori, M. (2019).

Carcinogenic and non-carcinogenic health risk assessment of heavy metals in drinking water of Khorramabad, Iran. *Methods X*, *6*, 1642-1651.

Mohanadas, D., Rohani, R., Sulaiman, Y., Bakar, S. A., Mahmoudi, E., & Zhang, L. C. (2023). Heavy metal detection in water using MXene and its composites: A review. *Materials Today Sustainability*, *22*, 100411.

Mwegoha, W., & Kihampa, C. (2010). Heavy metal contamination in agricultural soils and water in Dar es Salaam city, Tanzania. *African Journal of Environmental Science and Technology*, *4*(11), 763-769.

Nkinda, M. S., Rwiza, M. J., Ijumba, J. N., & Njau, K. N. (2021). Heavy metals risk assessment of water and sediments collected from selected river tributaries of the Mara River in Tanzania. *Discover Water*, *1*(1), 3.

Oginawati, K., Yapfrine, S. J., Fahimah, N., Salami, I. R. S., & Susetyo, S. H. (2023). The associations of heavy metals exposure in water sources to the risk of stunting cases. *Emerging Contaminants*, *9*(4), 100247.

Okafor, V. N., Omokpariola, D. O., Obumselu, O. F., & Eze, C. G. (2023). Exposure risk to heavy metals through surface and groundwater used for drinking and household activities in Ifite Ogwari, Southeastern Nigeria. *Applied Water Science*, *13*(4), 105.

Ozoko, D. C., Onyekwelu, I. L., & Aghamelu, O. P. (2022). Multivariate and health risks analysis of heavy metals in natural water sources around Enugu dumpsite, southeastern Nigeria. *Applied Water Science*, *12*(9), 224.

Peng, Q., Liu, L., Luo, Y., Zhang, Y., Tan, W., Liu, F., Suib, S. L., & Qiu, G. (2016). Cadmium removal from aqueous solution by a deionization supercapacitor with a birnessite electrode. *ACS Applied Materials & Interfaces*, *8*(50), 34405-34413.

Purkayastha, D., & Sarkar, S. (2020). Physicochemical structure analysis of chitin extracted from pupa exuviae and dead imago of wild black soldier fly (*Hermetia illucens*). *Journal of Polymers and the Environment*, *28*, 445-457.

Pyrzynska, K. (2019). Removal of cadmium from wastewaters with low-cost adsorbents. *Journal of Environmental Chemical Engineering*, *7*(1), 102795.

Qian, H., Yin, D., Qin, B., Li, L., Zhu, J., Mu, L., Li, C., Dong, B., Huang, D., & Lu, X. (2022). doped activated mesoporous carbon derived from the Borassus flabellifer flower as active electrodes for supercapacitors. *Materials Chemistry and Physics*, *240*, 122151.

Ramalingam, R. J., Sivachidambaram, M., Vijaya, J. J., Al-Lohedan, H. A., & Muthumareeswaran, M. (2020). Synthesis of porous activated carbon powder formation from fruit peel and cow dung waste for modified electrode fabrication and application. *Biomass and Bioenergy*, *142*, 105800.

Rangaraj, V. M., Edathil, A. A., Kannangara, Y. Y., Song, J. K., Haija, M. A., & Banat, F. (2019). Tamarind shell derived N-doped carbon for capacitive deionization studies. *Journal of Electroanalytical Chemistry*, *848*, 113307.

Rao, H. J. (2021). Characterization Studies on Adsorption of Lead and Cadmium using Activated Carbon Prepared from Waste Tyres. *Nature Environment & Pollution Technology*, *20*(2), 1-8.

Ratchai, E., Luengchavanon, M., Techato, K. A., Limbut, W., Chotikhun, A., & Voo, N. Y. (2023). Characteristics of Carbon from Chitin-coated $LiFePO_4$ and its Performance for Lithium Ion Battery. *BioResources*, 18(3), 4399.

Ravanipour, M., Hadi, M., Rastkari, N., Hemmati-Borji, S., & Nasseri, S. (2021). Presence of heavy metals in drinking water resources of Iran: A systematic review and meta-analysis. *Environmental Science and Pollution Research*, *28*, 26223-26251.

Ruibin, Q., Zhongai, H., Yuying, Y., Zhimin, L., Ning, A., Xiaoying, R., Haixiong, H., & Hongying, W. (2015). Monodisperse carbon microspheres derived from potato starch for asymmetric supercapacitors. *Electrochimica Acta*, *167*, 303-310.

Rwiza, M. J., Mohammed, N. K., & Banzi, F. P. (2021). Health risk assessment of trace elements in soil for people living and working in a mining area. *Journal of Environmental and Public Health*, *2021*.

Sarwar, A., Ali, M., Khoja, A. H., Nawar, A., Waqas, A., Liaquat, R., Naqvi, S. R., & Asjid, M. (2021). Synthesis and characterization of biomass-derived surface-modified activated carbon for enhanced $CO_2$ adsorption. *Journal of $CO_2$ Utilization*, *46*, 101476. https://doi.org/https://doi.org/10.1016/j.jcou.2021.101476

Siddiqui, E., & Pandey, J. (2019). Assessment of heavy metal pollution in water and surface sediment and evaluation of ecological risks associated with sediment contamination in the Ganga River: A basin-scale study. *Environmental Science and Pollution Research, 26*, 10926-10940.

Soetemans, L., Uyttebroek, M., & Bastiaens, L. (2020). Characteristics of chitin extracted from black soldier fly in different life stages. *International Journal of Biological Macromolecules, 165*, 3206-3214.

Song, Z., Li, L., Chen, Y., Duan, X., & Ren, N. (2023). Efficient removal and recovery of $Cd^{2+}$ from aqueous solutions by capacitive deionization method using biochars. *Journal of Materials Science & Technology, 148*, 10-18.

Surendra, K. C., Takara, D., Hashimoto, A. G., & Khanal, S. K. (2014). Biogas as a sustainable energy source for developing countries: Opportunities and challenges. *Renewable and Sustainable Energy Reviews, 31*, 846-859.

Truong, Q. M., Nguyen, T. B., Chen, W. H., Chen, C. W., Patel, A. K., Bui, X. T., Singhania, R. R., & Dong, C. D. (2023). Removal of heavy metals from aqueous solutions by high performance capacitive deionization process using biochar derived from Sargassum hemiphyllum. *Bioresource Technology, 370*, 128524.

Tuli, F., Hossain, A., Kibria, A. F., Tareq, A., Mamun, S. M., & Ullah, A. A. (2020). Removal of methylene blue from water by low-cost activated carbon prepared from tea waste: A study of adsorption isotherm and kinetics. *Environmental Nanotechnology, Monitoring & Management, 14*, 100354.

Wang, C., Wang, J., Wu, W., Qian, J., Song, S., & Yue, Z. (2019). Feasibility of activated carbon derived from anaerobic digester residues for supercapacitors. *Journal of Power Sources, 412*, 683-688.

Wang, J. R., Wan, F., Lü, Q. F., Chen, F., & Lin, Q. (2018). Self-nitrogen-doped porous biochar derived from kapok (*Ceiba insignis*) fibers: Effect of pyrolysis temperature and high electrochemical performance. *Journal of Materials Science & Technology, 34*(10), 1959-1968.

Wang, L. L., Wu, J., Wang, Z. J., Li, W. Z., & Zhang, K. (2017). Effects of three biochars as adsorbents on soils adsorbing ammonium nitrogen in biogas slurry. *Journal of Chemistry*, *2017*(1), 4627928.

Wang, Q., Cao, Q., Wang, X., Jing, B., Kuang, H., & Zhou, L. (2013). A high-capacity carbon prepared from renewable chicken feather biopolymer for supercapacitors. *Journal of Power Sources*, *225*, 101-107.

Wang, R., Zhao, Y., Xu, C., Liu, Y., Wu, W., & Zhao, D. (2024). Enhanced removal of $Pb^{2+}$, $Cd^{2+}$ and $Zn^{2+}$ ions on porous carbon from aqueous solutions by capacitive deionization: Performance study and underlying mechanism. *Surfaces and Interfaces*, *45*, 103858. https://doi.org/https://doi.org/10.1016/j.surfin.2024.103858

Wang, Z., Su, Q., Wang, S., Gao, Z., & Liu, J. (2021). Spatial distribution and health risk assessment of dissolved heavy metals in groundwater of eastern China coastal zone. *Environmental Pollution*, *290*, 118016.

Waśko, A., Bulak, P., Polak-Berecka, M., Nowak, K., Polakowski, C., & Bieganowski, A. (2016). The first report of the physicochemical structure of chitin isolated from Hermetia illucens. *International Journal of Biological Macromolecules*, *92*, 316-320.

Wu, J., Wang, T., Wang, J., Zhang, Y., & Pan, W. P. (2021). A novel modified method for the efficient removal of Pb and Cd from wastewater by biochar: Enhanced the ion exchange and precipitation capacity. *Science of the Total Environment*, *754*, 142150.

Xu, P., Elson, B., & Drewes, J. E. (2014). Electrosorption of heavy metals with capacitive deionization: Water reuse, desalination and resources recovery. *Desalination: Water from Water*, 2014, 521-548.

Xu, Y., Zhong, Z., Zeng, X., Zhao, Y., Deng, W., & Chen, Y. (2023). Novel materials for heavy metal removal in capacitive deionization. *Applied Sciences*, *13*(9), 5635.

Ye, P., Qin, L., He, M., Wu, F., Chen, Z., Liang, M., & Deng, L. (2025). Potential of zero charge-mediated electrochemical capture of cadmium ions from wastewater by lotus leaf-derived porous carbons. *Acta Physico-Chimica Sinica*, *41*(3), 100023.

Yin, T., Zhang, Y., Dong, D., Wang, T., & Wang, J. (2022). Highly efficient capacitive removal of $Cd^{2+}$ over $MoS_2$-Carbon framework composite material in desulphurisation wastewater from coal-fired power plants. *Journal of Cleaner Production*, *355*, 131814.

Younes, I., & Rinaudo, M. (2015). Chitin and chitosan preparation from marine sources. Structure, properties and applications. *Marine Drugs*, *13*(3), 1133-1174.

Yuan, X., Shi, X., Zeng, S., & Wei, Y. (2011). Activated carbons prepared from biogas residue: Characterization and methylene blue adsorption capacity. *Journal of Chemical Technology & Biotechnology*, *86*(3), 361-366.

Zargar, V., Asghari, M., & Dashti, A. (2015). A review on chitin and chitosan polymers: Structure, chemistry, solubility, derivatives, and applications. *ChemBioEng Reviews*, *2*(3), 204-226.

Zhang, M., Tang, Z., Zhao, Y., Wang, X., & Xu, X. (2020). *Study on the Adsorption Properties of Different Insect Feces on $Cu^{2+}$ and $Cd^{2+}$. In IOP Conference Series: Earth and Environmental Science (Vol. 450, No. 1, p. 012124)*. https://scholar.google.com

Zhang, Y., Chu, C., Li, T., Xu, S., Liu, L., & Ju, M. (2017). A water quality management strategy for regionally protected water through health risk assessment and spatial distribution of heavy metal pollution in 3 marine reserves. *Science of the Total Environment*, *599*, 721-731.

Zhang, Y., Liu, S., Zheng, X., Wang, X., Xu, Y., Tang, H., Kang, F., Yang, Q. H., & Luo, J. (2017). Biomass organs control the porosity of their pyrolyzed carbon. *Advanced Functional Materials*, *27*(3), 1604687.

Zhang, Y., Xue, Q., Li, F., & Dai, J. (2019). Removal of heavy metal ions from wastewater by capacitive deionization using polypyrrole/chitosan composite electrode. *Adsorption Science & Technology*, *37*(3-4), 205-216.

Zhao, C., Liu, G., Sun, N., Zhang, X., Wang, G., Zhang, Y., Zhang, H., & Zhao, H. (2018). Converting eggplant biomass into multifunctional porous carbon electrodes for self-powered capacitive deionization. *Environmental Science: Water Research & Technology*, *5*(6), 1054-1063.

Zhao, L., Li, Y., Yu, M., Peng, Y., & Ran, F. (2023). Electrolyte-wettability issues and challenges of electrode materials in electrochemical energy storage, energy conversion, and beyond. *Advanced Science*, *10*(17), 2300283.

Zhu, H., Tan, X., Tan, L., Chen, C., Alharbi, N. S., Hayat, T., Fang, M., & Wang, X. (2018). Biochar derived from sawdust embedded with molybdenum disulfide for highly selective removal of $Pb^{2+}$. *ACS Applied Nano Materials*, *1*(6), 2689-2698.

## RESEARCH OUTPUTS

### (i) Publication

Panja, E., Alfredy, T., Elisadiki, J., & Jande, Y. A. (2025). *Hermetia illucens* pupae casings and biogas slurry activated carbon electrodes for $Cd^{2+}$ removal from aqueous solutions using capacitive deionization. *Desalination and Water Treatment*, *322*, 101118.

### (ii) Poster presentation